©2004 by Economic Geology
Vol. 99, pp. 3–37

Henderson Porphyry Molybdenum System, Colorado: I. Sequence and Abundance of Hydrothermal Mineral Assemblages, Flow Paths of Evolving Fluids, and Evolutionary Style

Eric Seedorff†

Center for Mineral Resources, Department of Geosciences, 1040 East Fourth Street, University of Arizona, Tucson, Arizona 85721-0077

and Marco T. Einaudi

Department of Geological and Environmental Sciences, Stanford University, Stanford, California 94305-2115

Abstract

At Henderson, Colorado, 12 rhyolitic stocks of Oligocene age crystallized in three intrusive centers whose tops are 1 km below the surface of Red Mountain: Henderson (oldest), Seriate, and Vasquez (deepest and youngest). A variety of fluorine-rich hydrothermal mineral assemblages are grouped according to their temperatures of formation, either high-, moderately high, moderate-, or low-temperature (the latter three groups are termed lower temperature assemblages). The groupings were based on relative age relationships in areas free of cyclical events, and absolute temperature estimates based on fluid inclusion study later were made for many mineral assemblages, as detailed in a companion paper. Numerous crosscutting contacts of individual stocks combined with limits of associated high-temperature assemblages can be interpreted as spatially extensive time lines, thereby enabling temporal correlation of spatially separated events. High-temperature silicic (quartz-fluorite) and intense potassic (quartz-K-feldspar-molybdenite) assemblages developed in numerous cycles, each corresponding to emplacement of a stock and deposition of molybdenite. Molybdenite occurs without pyrite mostly in the high-temperature assemblages. In contrast, lower temperature assemblages broadly envelop intrusive centers, rather than single stocks. Some of the moderately high temperature, less intense potassic assemblages (including mottled K-feldspar-quartz and magnetite-K-feldspar) also formed during multiple cycles. Moderate-temperature sericitic assemblages (including topaz with pyrite or magnetite and sericite with pyrite or magnetite) only locally exhibit evidence for multiple cycles, and low-temperature intermediate argillic assemblages (pyrite-clay and several assemblages containing base metal sulfides, F-bearing, Mn-rich garnet, and rhodochrosite) were deposited in only a single event. These lower temperature assemblages terminate 700 m below the present surface. A zone of relatively fresh rocks extends upward and outward from this termination, separating the lower temperature assemblages from the first appearance of propylitic alteration in a more peripheral position, beyond the area of study. At no time did an advanced argillic assemblage form.

Lower temperature assemblages are subdivided into two suites on the basis of position: above intrusive centers, formed from fluids that flowed upward out the top of mineralizing stocks from several intrusive centers; and on the flanks of the Seriate center, formed from fluids released from the apex of the Seriate stock and injected laterally and downward along the flanks of the stock. Na- and Na-K-feldspars (± K-feldspar ± topaz ± micas) are members of some assemblages of the second suite.

The upper and lower limits of the hydrothermal system, for much of its history, are preserved within the exposures studied. The upper limit of the hydrothermal system rose to 250 m above the apices of the stocks for the first time during development of low-temperature assemblages, which extended higher above Henderson than Seriate. Prior to that time, the region where thermally and chemically evolving, saline hydrothermal fluid was reacting with wall rocks was confined to a vertical interval of approximately 0.5 km. The base of the system rose as moderately high and moderate-temperature assemblages formed but fell rapidly in elevation upon development of low-temperature assemblages. There is no evidence for system-scale convective circulation of fluids during development of the assemblages studied. Sericitic alteration did not begin to form anywhere in the system until after intense potassic alteration had terminated in the vicinity of stocks in both the Henderson and Seriate centers; proximal to stocks, the multiplicity of intrusive events repeatedly reversed the overall trend toward lower temperatures. Sericitic alteration was followed by a late cycle of intense potassic alteration and molybdenite deposition associated with emplacement and crystallization of the Vasquez stock prior to formation of low-temperature assemblages.

The hydrothermal system that formed the Henderson orebody can be viewed as a series of thermally retrograding cycles, all except the last of which was truncated by a reversal in the general trend of declining temperatures. Hence, the evolutionary style of Henderson is termed variably cyclical, in contrast to the nearly perfectly cyclical style embodied in the original Climax model for porphyry molybdenum deposits and the nearly perfectly unidirectional style envisaged for many porphyry copper deposits. An evaluation of evolutionary style can lead to geologic tests for geochronologic interpretations and proposed genetic origins of deposits.

† Corresponding author: e-mail, seedorff@geo.arizona.edu

Introduction

ALTHOUGH Wallace et al. (1968) developed a cyclical model for the Climax porphyry molybdenum deposit and Gustafson (1978) suggested that some porphyry copper deposits display reversals in evolutionary trend, the common view developed that porphyry systems evolve largely unidirectionally from early potassic alteration at high temperatures to later sericitic alteration at lower temperatures. For decades, this view was equated with a shift in origin of hydrothermal fluids from magmatic to dominantly meteoric (Sheppard et al., 1971; Gustafson and Hunt, 1975; Einaudi, 1977, 1982; Beane, 1983; Beane and Bodnar, 1995; Gustafson and Quiroga G., 1995; Taylor, 1997), although fluids with a dominantly magmatic origin recently have been identified as constituting a larger fraction of the history of porphyry systems (e.g., Hedenquist et al., 1998; Zhang et al., 1999; Ulrich et al., 2001; Watanabe and Hedenquist, 2001; Harris and Golding, 2002).

Simplified depictions of alteration and mineralization shown in review papers on porphyry deposits, such as the morphology of ore shells and distribution of alteration zones (e.g., Guilbert and Lowell, 1974; Rose and Burt, 1979; McMillan and Panteleyev, 1995; Sillitoe, 2000), are of limited use in developing an understanding of processes. With a few outstanding exceptions (e.g., Gustafson and Hunt, 1975; Carten, 1986; Carten et al., 1988b; Dilles and Einaudi, 1992; Gustafson and Quiroga G., 1995; Arancibia and Clark, 1996; Muntean and Einaudi, 2000, 2001), papers on individual deposits contain little detail regarding temporal aspects of alteration-mineralization (cf. Gustafson, 1978), and field data generally have been recorded in terms of the spatial distribution of alteration zones or alteration types, rather than in terms of the succession and abundance of mineral assemblages and vein types.

Certain genetic aspects of the porphyry system at Henderson are more tightly constrained than in any porphyry copper system, including those that are well exposed by postmineral tilting and/or deep drilling and that are well mapped and documented, such as Yerington and Ann-Mason, Nevada (Proffett and Dilles, 1984, Carten, 1986; Dilles and Einaudi, 1992; Dilles et al., 2000) and El Salvador, Chile (Gustafson and Hunt, 1975; Gustafson and Quiroga G., 1995; Gustafson et al., 2001). Recognizing these constraints was possible at Henderson because it (1) is free of supergene alteration; (2) is compact in size and exceptionally exposed by drilling and drifting; (3) has spatially extensive, crosscutting contacts of numerous intrusions that can be used to infer time lines; and (4) exhibits abundant mineralogic evidence of fluid evolution, coupled with relatively fresh rocks exposed at both shallow and deep levels of the system. In this paper we use the data on succession and abundance of mineral phases to address such questions as the timing of initiation of alteration at high levels in the system (e.g., sericitic) relative to termination of alteration at deep levels (e.g., potassic), and the relative importance of multiple and cyclical hydrothermal processes versus unidirectional evolution. We show that ephemeral features of hydrothermal systems, which bear on important genetic questions, are well preserved at Henderson and reveal more of the detail and complexity of porphyry systems than is portrayed either by descriptive and genetic models (Gustafson and Hunt, 1975; Burnham, 1979; Burnham and Ohmoto, 1980; Titley and Beane, 1981; White et al., 1981; Giggenbach, 1997; Hedenquist and Richards, 1998; Fournier, 1999) or by theoretical and numerical models (Helgeson, 1970; Cathles, 1977; Henley and McNabb, 1978; Brimhall, 1980; Norton, 1982; Cline and Bodnar, 1991; Cline, 1995).

This paper builds on earlier investigations conducted while Henderson was being explored and developed (MacKenzie, 1970; Ranta et al., 1976; Wallace et al., 1978; Gunow et al., 1980; White et al., 1981) and on studies of the structural setting, age, textures, and compositions of intrusive rocks, and high-temperature alteration-mineralization by mine geologists and collaborators (Shannon et al., 1982; Carten et al., 1988a, b; Geraghty et al., 1988; Geissman et al., 1992). Carten et al. (1988a, b) described the cyclical development at Henderson of silicic and intense potassic alteration at high temperatures. In this paper we focus on the evolution of the hydrothermal system at lower temperatures. Our purposes are (1) to document the hydrothermal mineral assemblages, the compositions of selected hydrothermal minerals as a function of assemblage, and the sequence and abundance of assemblages; (2) to identify the flow paths of progressively evolving fluids; (3) to deduce the overall history of the hydrothermal system; (4) to place the evolution of the Henderson system in the context of other well-studied porphyry deposits; and (5) to illustrate how characterization of evolutionary style can be used to address ore genesis. A companion paper (Seedorff and Einaudi, 2004) describes the changing chemical and physical environment of fluids in this context and the consequences for introduction and deposition of metals.

Geologic Setting and Intrusive History

Henderson and Urad constitute a stacked pair of Climax-type porphyry molybdenum deposits that are associated with Oligocene high-silica rhyolite intrusions at Red Mountain, Dailey-Jones Pass mining district, in the Front Range of the Rocky Mountains, Colorado (Wallace et al., 1978; White et al., 1981; Carten et al., 1988b, 1993; Geissman et al., 1992; Carten and Snee, 1995; Wallace, 1995). The older, shallower, and much smaller Urad deposit (Fig. 1) is related to the Square Quartz porphyry (Wallace, 1974; Wallace et al., 1978) and hosted by three stocks of Oligocene rhyolite porphyry and wall rock of Silver Plume Granite, a composite batholith of biotite-muscovite granite of Middle Proterozoic age (1.4 Ga; Peterman et al., 1968). The mined-out Urad deposit produced 12 million metric tons (Mt) of ore at an average grade of 0.35 percent MoS_2 (Carten et al., 1993).

The Urad deposit is cut off by a cylindrical intrusion, the Red Mountain porphyry, which probably vented to the surface (Wallace et al., 1978, p. 337, 342; Stein and Crock, 1990, p. 200). The Red Mountain porphyry flares out at depth into a larger body, the Urad porphyry (Fig. 1).

The Henderson deposit is associated with a dozen or more, small, texturally and compositionally zoned stocks, none of which vented to the surface (Carten et al., 1988a, b), which intrude the Urad porphyry (Fig. 1). The stocks are grouped into three closely spaced intrusive centers (Figs. 2–5): from oldest to youngest, the Henderson, Seriate, and Vasquez centers. The stocks are biotite high-silica rhyolites with unusual accessory minerals and highly evolved chemical compositions

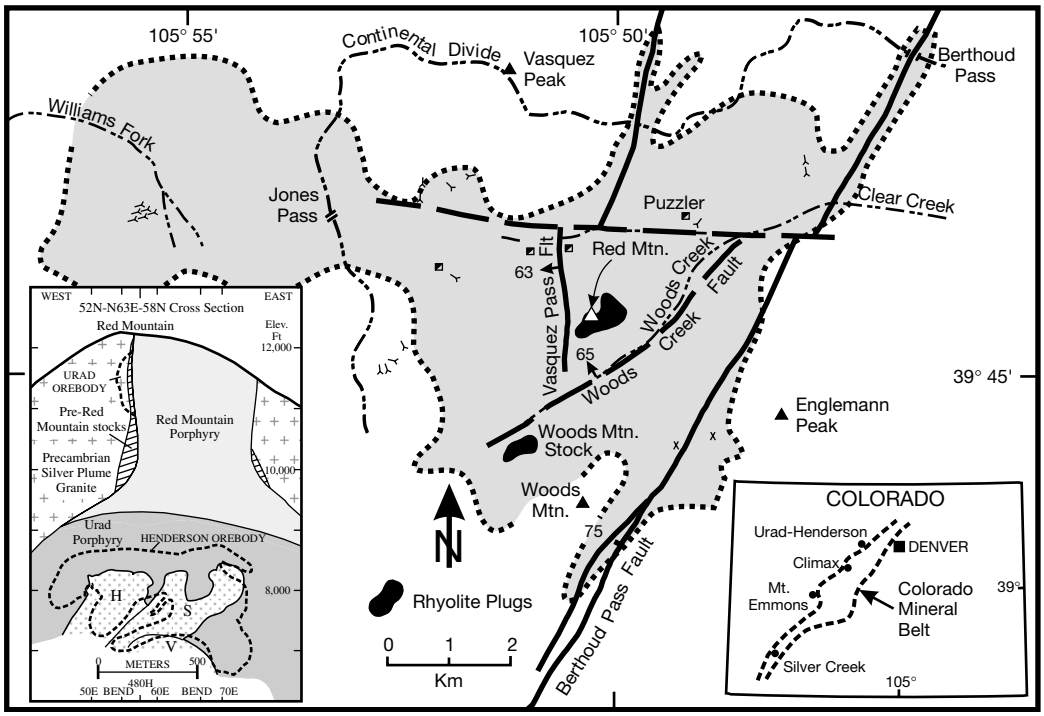

FIG. 1. Simplified geologic map of the Dailey-Jones Pass mining district, with inset maps showing the location of Henderson in the state of Colorado and a cross section through Red Mountain. Map shows outline of propylitic alteration, which is a composite feature in part related to hydrothermal systems at Red Mountain (R. B. Carten, pers. commun., 2001). The inset cross section (see Fig. 3 for location) looks north and shows pre-Red Mountain porphyry stocks that are broadly related to the Urad orebody and porphyries that postdate crystallization of the texturally zoned Red Mountain/Urad porphyry that are broadly related to the Henderson orebody. The latter can be subdivided into the Henderson (H), Seriate (S), and Vasquez (V) intrusive centers. Map is based on Wallace et al. (1978, fig. 3), Geraghty et al. (1988, fig. 1), Geissman et al. (1992, fig. 1), and R. B. Carten (pers. commun., 1985).

(Desborough and Mihalik, 1980; Carten et al., 1988a, b, 1993). The stocks and the surrounding Urad porphyry together constitute a nearly uniform, iron-poor physical and chemical environment, such that variability in host-rock composition could not have significantly affected the patterns of hydrothermal mineral assemblages. Although individual stocks display pronounced textural zonation (Carten et al., 1988b, Figs. 2–3, 7, 9–10) that was recorded during core logging, the locations of these internal contacts are not important to this study.

The Henderson orebody consists of three overlapping ore zones, each of which is associated with one of the intrusive centers (Figs. 2, 4). The three ore zones are themselves composite (Figs. 2–3), because each individual stock developed its own ore shell (Carten et al., 1988a, b). The Henderson intrusive center is composed of five stocks—the Phantom, Berthoud, Henderson, Primos, and Arapaho porphyries, as well as several prominent dikes and a breccia body (Figs. 2–3; see also Carten et al., 1988b, p. 271–272). The focus of intrusion subsequently moved to the east-northeast, where stocks of the Seriate center (East Lobe, Seriate, Ruby, and Nystrom) were emplaced, and finally shifted to deeper levels, where stocks of the Vasquez center (Vasquez, Dailey, and Ute) crystallized.

In spite of the compact size of the Henderson system, Henderson is the second largest deposit of the Climax type, with combined production and reserves of 437 Mt of ore at an average grade of 0.38 percent MoS_2, using a cut-off grade of 0.2 percent MoS_2 (table 1, fig. 5 of Carten et al., 1993). A rough geologic inventory to the limit of observed molybdenite adds only a few tens of percent to the total mass of molybdenum in the system because of the tight spacing of grade isopleths (Fig. 2B).

The Henderson and Urad deposits occur within an intact structural block (Fig. 1) bounded on the west by the postore Vasquez Pass fault and on the southeast by the Woods Creek fault (Geraghty et al., 1988). The entire block was tilted 15° to 25° east-southeast concurrent with opening of the Rio Grande rift (Geraghty et al., 1988; Geissman et al., 1992).

Methods

Field data were collected by logging approximately 15,000 m of core, the vast majority of which is within 45 m of two vertical sections that were selected for detailed study (Fig. 3; drill hole locations shown in figs. 3 and 4 of Seedorff, 1988). The abundance of each mineral assemblage (prior to any changes in mineralogy produced by later, superimposed events) was recorded in volume percent for each 10-ft interval of core on the basis of visual estimates from hand lens examination and petrographic study (Seedorff, 1987, app. A. Two hundred fifty thin sections (mostly polished) were described by petrographic examination under transmitted and reflected light.

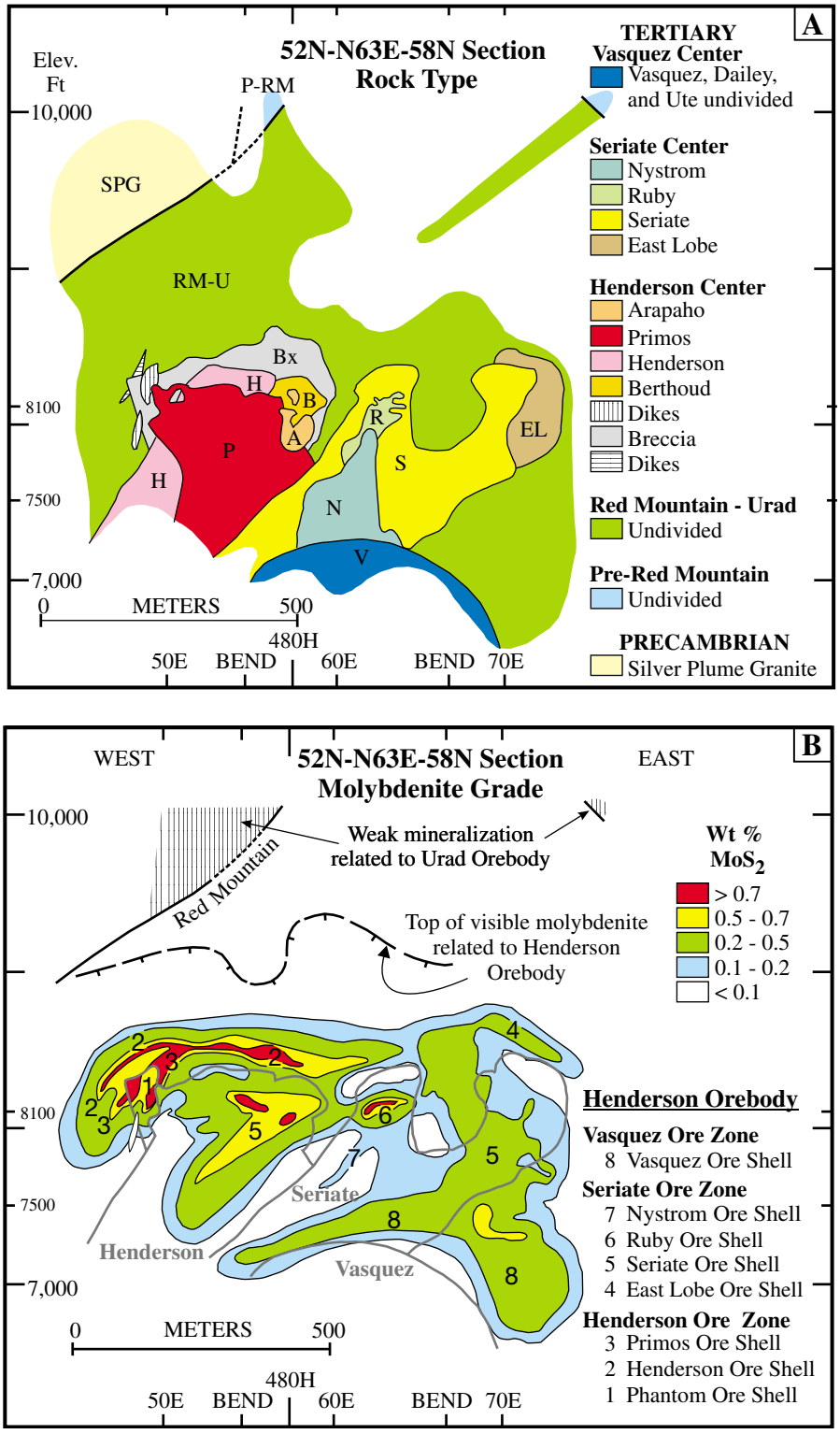

FIG. 2. Simplified distribution of rock types and molybdenite grade in cross section 52N-N63E-58N. The central panel of the bent section is oriented along the axis of intrusion, and most stocks (except Arapaho) are nearly bisected by the section (see Fig. 3 for location). A. Stocks related to the Henderson orebody define three intrusive centers; clockwise from upper left they are the Henderson, Seriate, and Vasquez. Only the outlines of intrusive centers appear in most subsequent figures. The colored regions indicate the extent of exposure by drill holes. B. Molybdenite grade distribution with gray lines outlining intrusive centers. Three broad, overlapping ore zones, each related to a separate intrusive center, are visible. In detail, however, this section displays eight ore shells of various shapes, each related to a separate stock (compare to A). Low-grade holes centered on the apices of the Henderson and Seriate stocks (compare to A) are the sites of the two high silica zones.

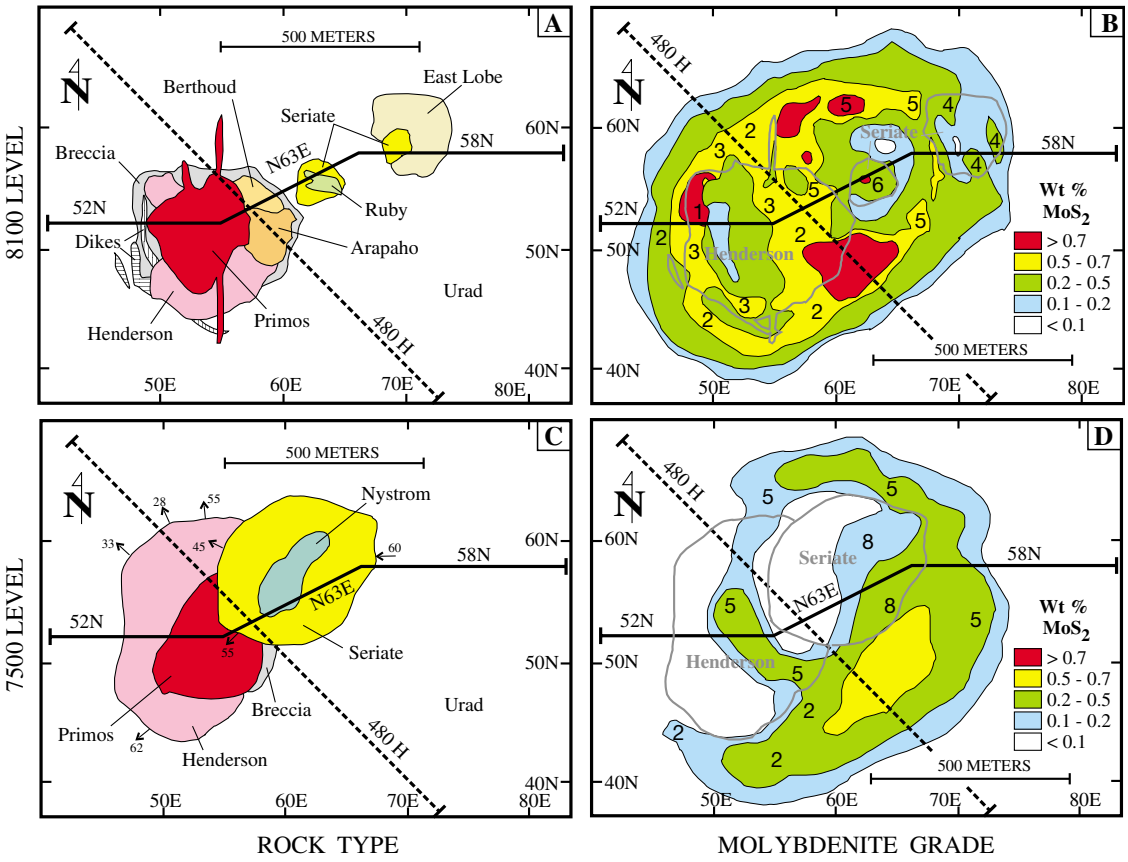

FIG. 3. Geologic maps and molybdenite grade distributions on 8100 and 7500 levels (approx elevation in feet above sea level; see Fig. 2) of the Henderson mine, showing lines of section. Gray lines in (B) and (D) outline intrusive centers. Ore shells related to individual stocks are numbered (see legend of Fig. 2B for key); overlap of ore shells contributes to higher grades. A. Rock types on 8100 level, showing apices of stocks of the Henderson and Seriate centers. B. Molybdenite grade distribution on 8100 level. Ore shells related to Phantom, Henderson, and Primos stocks of the Henderson center and East Lobe, Seriate, and Ruby stocks of the Seriate center are present on this level, as are several places where grades are truncated by intrusive contacts. C. Rock types on 7500 level, showing deeper levels of several stocks of Henderson and Seriate intrusive centers. D. Molybdenite grade distribution on the 7500 level, where moderate east-southeast tilting of the Henderson orebody is apparent. Ore shells related to the Henderson and Seriate stocks form claw- to ring-shaped patterns, with slight truncation of the Henderson shell at the contact with the Seriate stock. The upper part of the domal Vasquez ore shell, related to the underlying Vasquez stock in the center of the map (see Fig. 2), contributes >0.1 percent MoS_2 in the eastern half of the Seriate stock and adjacent areas of Urad porphyry. Thus, the highest grade area on this level is a composite of three ore shells.

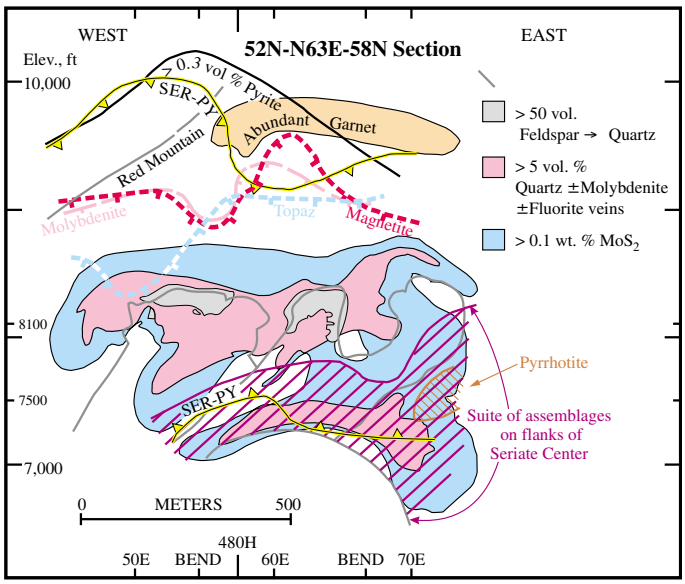

FIG. 4. Simplified present-day view of selected alteration-mineralization characteristics of the Henderson deposit along section 52N-N63E-58N, with gray lines outlining intrusive centers. One contour of intensity of high-temperature silicic alteration is shown, which outlines two areas where >50 vol percent of feldspar is replaced by quartz (centered on apices of Henderson and Seriate stocks). Compared to intense silicic alteration, the limit of >5 vol percent quartz ± fluorite ± molybdenite veins, the outline of greater than 0.1 wt percent MoS_2, and the upper limit of molybdenite, which corresponds to approximately 0.007 to 0.015 percent MoS_2, represent progressively more distal effects, respectively, of high-temperature alteration-mineralization. Moderately high- and moderate-temperature mineral assemblages produce upper limits of magnetite and topaz. Both upper and lower limits of the pyrite-bearing, moderate-temperature, sericitic assemblage (SER-PY) are exposed. Distribution of pyrrhotite, abundant garnet, and contour of >0.3 vol percent pyrite are controlled primarily by distribution of low-temperature assemblages. The inner limit of propylitic alteration is beyond the area shown in this cross section.

Crosscutting relationships between intrusions and veins and offsetting relationships between different veins were observed and recorded. Caution was exercised in interpreting potentially deceptive exposures, such as cases where younger veinlets fill reopened older veinlets and failure of veinlets to deposit minerals (especially feldspars and sulfides) where they crosscut chemically unfavorable hosts (e.g., quartz). Logging results were compiled, and the abundance of each mineral assemblage was visually smoothed and contoured, with due regard for discontinuities created by intrusive contacts that cut off veins. Crosscutting relationships and spatial distributions were used to strip off younger events, one at a time, to illustrate the temporal evolution of the hydrothermal system, (Seedorff, 1987, app. A; 1988), illustrated here for section 52N-N63E-58N (Fig. 2).

Compositions of feldspar, biotite, topaz, sericite and/or muscovite, garnet, and wolframite from various hydrothermal mineral assemblages were determined by wavelength-dispersive electron microprobe (JEOL 733A Superprobe) analysis in polished thin sections by standard techniques (Seedorff, 1987, apps. B and D), supplemented by analyses from an energy dispersive spectrometer (EDS) to aid mineral identification. Certain assemblages contain trace amounts of heavy oxide minerals such as W- and Sn-bearing ilmenorutile, (Ti, Nb, Ta, Fe^{3+}, Fe^{2+})O_2, whose compositions are documented by Gunow (1983). A reconnaissance survey of clay mineral identifications utilized a portable short-wave infrared spectrometer (PIMA™).

Hydrothermal Mineral Assemblages

Definitions

The term assemblage herein specifies a group of minerals, including metal-bearing phases, which appear to be stable together at the mesoscopic scale and to have formed contemporaneously. The plus symbol (+) links minerals that everywhere are present in the assemblage and the plus or minus symbol (±) precedes minerals that are not everywhere present. Minerals that are uncommon in the assemblage or present in only trace amounts are enclosed in parentheses. Relict but stable magmatic minerals are included in the definition, but at Henderson magmatic minerals other than quartz are destroyed or changed in composition by alteration. The complete mineral assemblage is represented by a short abbreviation (shown in all-capital letters), which uses abbreviations for key minerals in the assemblage, as listed in Table 1.

TABLE 1. Lower Temperature Assemblages

Group	Assemblage[1]	Abbreviation[2,3]
Moderately high temperature	Brown biotite ± K-feldspar ± K-Na feldspar ± Na feldspar ± quartz ± fluorite ± magnetite ± molybdenite ± (topaz ± rutile)	BIO-KSP*
	Quartz + topaz + magnetite + brown biotite ± K-feldspar ± K-Na feldspar ± Na feldspar ± fluorite ± (garnet ± molybdenite ± rutile ± wolframite ± ilmenorutile)	TPZ-BIO-MT*
	K-feldspar + quartz ± (molybdenite ± brown biotite ± fluorite ± rutile)	MOTTLED KSP-QTZ
	Magnetite ± K-feldspar ± quartz ± fluorite ± (molybdenite ± brown biotite ± topaz ± muscovite ± rutile)	MT-KSP
Moderate temperature	Quartz + topaz + magnetite ± K-feldspar ± garnet ± (fluorite ± rutile)	TPZ-MT*
	Quartz + sericite (or muscovite) + magnetite ± (Na feldspar ± fluorite ± rutile ± garnet ± ilmenorutile)	SER-MT*
	Quartz + green biotite ± topaz ± fluorite ± pyrite [or magnetite instead of pyrite] ± sphalerite ± garnet ± (sericite ± rutile ± ilmenorutile)	GREEN BIO*
	Quartz + topaz + pyrite ± fluorite ± wolframite ± (rutile ± garnet ± ilmenorutile)	TPZ-PY
	Quartz + sericite + pyrite + (rutile ± fluorite ± garnet ± wolframite)	SER-PY
Low temperature	Pyrrhotite ± quartz? ± fluorite? + clay? [or sericite? or green biotite?] ± (rutile)	PO*
	Pyrite ± quartz ± clay ± fluorite ± (hematite ± garnet ± rhodochrosite ± rutile)	PY-CLAY
	Sphalerite ± pyrite ± quartz ± galena ± clay ± hematite ± (rutile ± chalcopyrite ± fluorite ± barite ± rhodochrosite?)	SPHAL
	Garnet ± sphalerite ± pyrite ± quartz ± galena ± clay ± (rutile ± chalcopyrite ± fluorite)	GAR
	Rhodochrosite ± pyrite ± fluorite ± clay ± (quartz ± leucoxene)	RHOD

[1] Terms used during logging of core: muscovite = pale-colored micas that are sufficiently coarse grained that individual grains are readily visible to the unaided eye; sericite = pale-colored, fine-grained phyllosilicates that occur in alteration envelopes which are fairly hard when scratched, that affect both K-feldspar and plagioclase sites, and that do not contain coexisting carbonate; clay = fine-grained phyllosilicates that occur in alteration envelopes that are fairly soft when scratched, which may contain carbonate and relict K-feldspar and tend to be grass green in color

[2] An asterisk (*) denotes a member of the suite of assemblages on the flanks of the Seriate center; the remaining assemblages are members of the suite of assemblages above intrusive centers

[3] Abbreviations for assemblages are based on the following abbreviations for minerals: BIO = biotite, GAR = garnet; GREEN BIO = green biotite, KSP = K-feldspar; MT = magnetite, PO = pyrrhotite, PY = pyrite QTZ = quartz, RHOD = rhodochrosite, SER = sericite, SPHAL = sphalerite, TPZ = topaz

Mineral assemblages are classified into alteration types (e.g., silicic, potassic, sericitic, and intermediate argillic) on the basis of similar physicochemical environments of formation (Meyer and Hemley, 1967, p. 167; Barton et al., 1991). Vein types are defined by the mineral assemblage(s) that occur in the vein filling and in the envelope of altered wall rock. Some vein types at Henderson exhibit zoned alteration envelopes (e.g., Meyer and Hemley, 1967, p. 180–183), with mineral assemblages that belong to more than one alteration type.

As traditionally defined and applied (e.g., Lowell and Guilbert, 1970; Rose, 1970; John, 1978; Ossandón et al., 2001), alteration and sulfide zones are deposit-scale regions that consist primarily of certain alteration or sulfide minerals, irrespective of whether they were deposited together. This usage of zonal terminology is abandoned here; rather, the spatial disposition of alteration-mineralization at the deposit scale is displayed in terms of the distribution and abundance of mineral assemblages that occur in vein fillings and altered wall rock. Within this deposit-scale distribution pattern, regions where an assemblage is especially abundant are referred to as zones of concentration or shortened to just zones. To the extent that certain ore minerals or metals are confined predominantly to one or two mineral assemblages, zones of concentration of certain mineral assemblages coincide broadly with the primary geochemical dispersion halos that produce molybdenum ore shells (Carten et al., 1988b) and minor and trace metal enrichment halos (Bright, 1974). An approximate correlation of the terminology of alteration zones of earlier workers with the presently defined space-time distribution of mineral assemblages can be found in Seedorff (1988).

The traditional terms that are used to group assemblages, such as early or main stage, lose their meaning in hydrothermal systems, such as Henderson, that are multicyclic. Consequently, assemblages herein are grouped by their temperatures of formation: high, moderately high, moderate, and low. These groupings were established on the basis of relative age relationships in areas free of cyclical events, leading to a temporal sequence from feldspar- and biotite-stable through sericite-stable assemblages, and ending with assemblages containing clay minerals, base metal sulfides, and carbonate. Lower temperature assemblages, which are the subject of this study, include all but the high-temperature assemblages. Based on interpretation of fluid inclusion data by Seedorff and Einaudi (2004), the range of temperatures for mineral assemblages in each group is as follows: moderately high, 600° to 460°C; moderate, 530° to 310°C; and low, 390° to 200°C.

Propylitic alteration, described by MacKenzie (1970), is absent in section 52N-N63E-58N (Figs. 3–5) but is present at high levels of the northwestern end of section 480 H (caption of Fig. 4; see also Seedorff, 1988). Propylitic alteration was excluded from detailed study, but one fluid inclusion run returned temperature estimates of 320° to 210°C (Seedorff and Einaudi, 2004). There is virtually no spatial overlap between propylitic alteration and the lower temperature assemblages described here.

Review of high-temperature assemblages

High-temperature mineral assemblages are spatially and genetically tied to crystallization of individual stocks (Carten et al., 1988a, b). The assemblages can be treated in terms of two simplified mineral assemblages that are related to veins filled with quartz + fluorite ± molybdenite (Figs. 4–5A): (1) a silicic type, quartz + fluorite ± (molybdenite), symbolized by QTZ-FL, and (2) an intense potassic type, K-feldspar + fluorite ± quartz ± molybdenite ± (brown biotite), symbolized by QTZ-KSP-MO (Fig. 5A; see Carten et al., 1988b, p. 284–289 for details). Near the apex of a stock, veinlets have low molybdenite contents and zoned envelopes of inner silicic and outer potassic alteration. In more distal positions, veinlets have higher molybdenite contents and only potassic envelopes. Where one mineralization event related to a single stock can be isolated, veins that have only potassic envelopes cut and offset veins that have zoned silicic-potassic envelopes. In some areas (Figs. 4–5A), inner silicic envelopes coalesce to form nearly pervasive silicic alteration (Carten et al., 1988b).

High-temperature veins formed contemporaneously along two sets of fractures around and within a given stock: a steeply dipping radial set and a moderately outward dipping, concentric set (table 4, fig. 12 of Carten et al., 1988b). The morphology of an ore shell at Henderson (Figs. 2–3) primarily reflects the net distribution, abundance, and molybdenite content of those two veins types (Carten et al., 1988b, p. 289, figs. 13–15), because nearly all molybdenite was deposited in the high-temperature veins and was not significantly remobilized by later events (Seedorff and Einaudi, 2004).

As shown by Carten et al. (1988b), high-temperature veins formed about a stock as the upper 200 m of the stock solidified, and each individual stock crystallized beyond the deepest levels of exposure before the high-temperature cycle of alteration-mineralization was repeated with the emplacement of the next intrusion in the center.

Lower temperature assemblages and types of veins

Patterns of distribution: The lower temperature assemblages (Table 1, revised from Seedorff, 1988) are subdivided into two suites on the basis of their spatial positions: most abundant above intrusive centers, and on the flanks of the Seriate center. The assemblages in the latter suite generally are best developed on the flanks of the Seriate center, but many assemblages in the suite also cut across the deep levels of the intrusive center (Figs. 4–5). The distribution and abundance of an assemblage depend on the sum of the distribution and abundance of the vein types that contribute to each assemblage; in some cases, a single assemblage is related to more than one major type of vein (Table 2). Photographs of selected lower temperature assemblages and associated veins are shown in Figure 6.

Compositions of hydrothermal minerals: Representative electron microprobe analyses of hydrothermal feldspar, mica, topaz, wolframite, and garnet from lower temperature assemblages are reported in Tables 3 to 5. The compositional ranges of selected hydrothermal minerals are summarized in Table 6. Although both igneous biotite and high-temperature hydrothermal biotite from Henderson are trioctahedral (R. B. Carten, unpub. data, 1986–1988; F. K. Mazdab and E. Seedorff, unpub. data, 2001), i.e., true biotites, none of the biotites of the lower temperature assemblages is trioctahedral. The latter biotites display wide variability between the ideal dioctahedral and trioctahedral subgroups (e.g., Bailey, 1984).

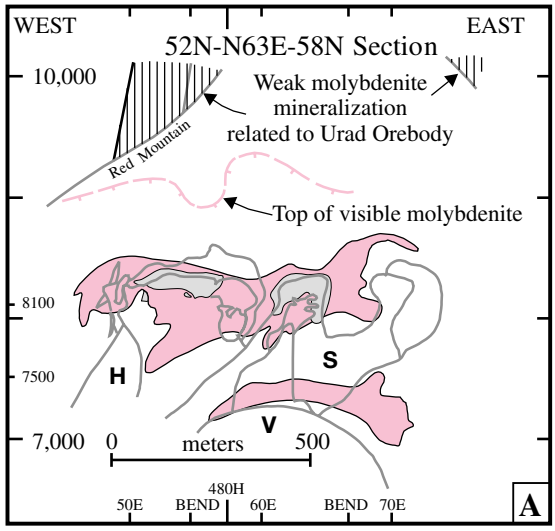

HIGH-TEMPERATURE ASSEMBLAGES

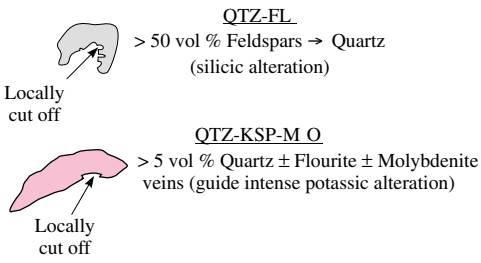

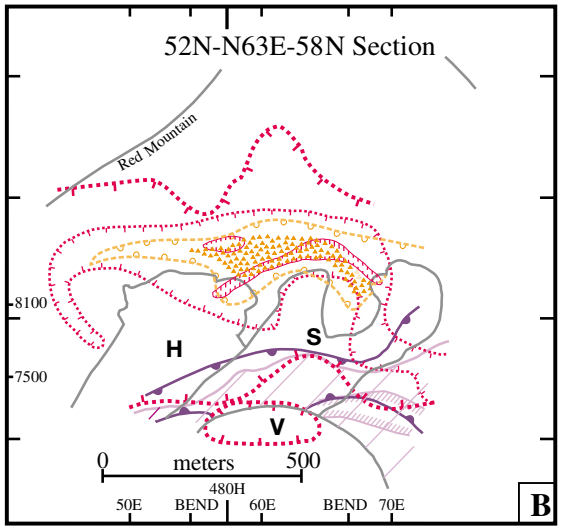

MODERATELY HIGH-TEMPERATURE ASSEMBLAGES

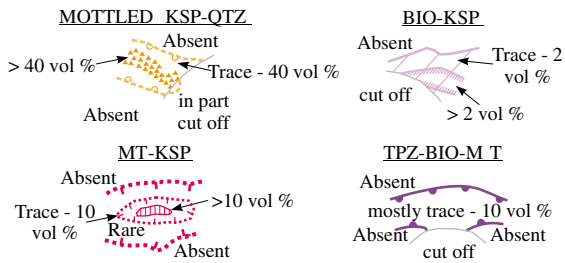

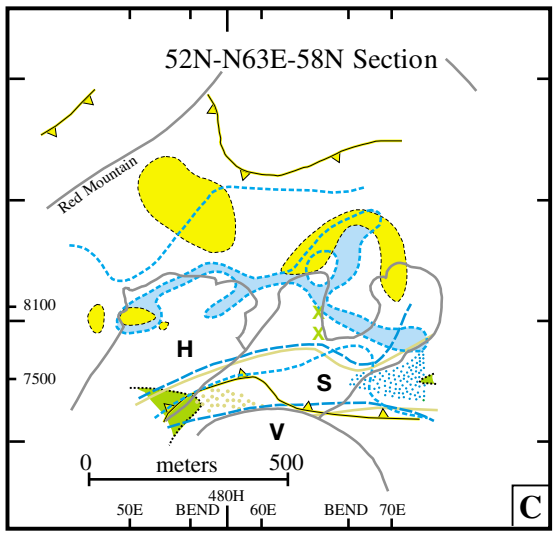

MODERATE-TEMPERATURE ASSEMBLAGES

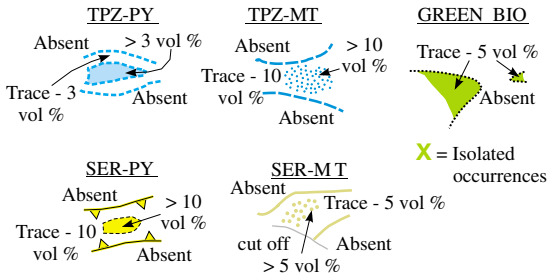

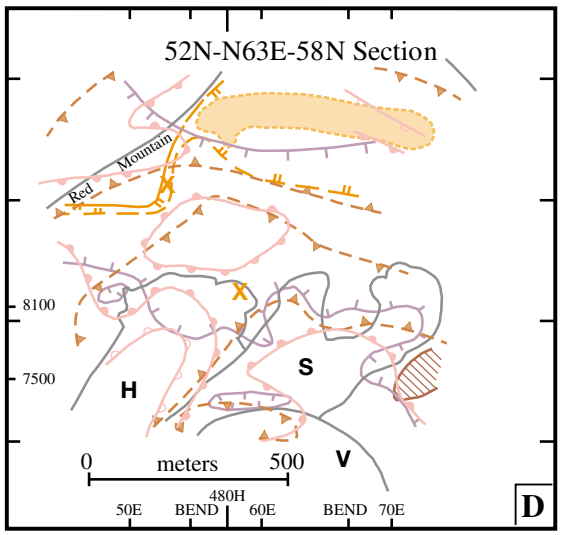

LOW-TEMPERATURE ASSEMBLAGES

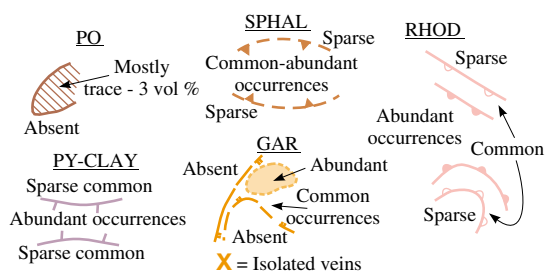

TABLE 2. Summary of Common Vein Types That Contribute to Lower Temperature Assemblages

Group	Assemblage[1]	Principal contributing vein types[2]	Widths[3] (mm)	Comments
Moderately high temperature	BIO-KSP*	BIO-KSP//BIO-KSP	0.2–3//0.4–10	Vein filling is commonly quartz rich
	TPZ-BIO-MT*	TPZ-BIO-MT//TPZ-BIO-MT	0–0.5//1–8	Commonly guided by sheeted sets of fractures
	MOTTLED KSP-QTZ	MOTTLED KSP-QTZ	0.05–0.4	Widths refer to widths of hairline veinlets
	MT-KSP	MT-KSP//MT-KSP	0.05–0.1//0.2–1	Commonly guided by discontinuous fractures
Moderate temperature	TPZ-MT*	TPZ-MT//TPZ-MT/SER-MT TPZ-MT//TPZ-MT	0.1–0.2//0.2–8/0.5–10 0–0.1//2–8	
	SER-MT*	SER-MT//SER-MT	0–0.3//2–8	Grain size of sericite typically is <0.01–0.1 mm; grain size of rare muscovite is 0.2–1.6 mm
		TPZ-MT//TPZ-MT/SER-MT	0.1–0.2//0.2–8/0.5–10	Grain size of sericite typically 0.02–0.1 mm
	GREEN BIO*	TPZ-PY//TPZ-PY/GREEN BIO GREEN BIO//GREEN BIO	0–5//0–10/5–10 0–0.5//1–5	
	TPZ-PY	TPZ-PY//TPZ-PY/SER-PY TPZ-PY//TPZ-PY/GREEN BIO	0.5–2//0.1–4/2–4 0–5//0–10/5–10	Generally through-going veinlets
	SER-PY	SER-PY//SER-PY	0–0.3//0.5–4	Grain size of sericite typically is <0.01–0.05 mm
		TPZ-PY//TPZ-PY/SER-PY	0.5–2//0.1–4/2–4	Grain size of sericite typically is <0.01–0.05 mm
Low temperature	PO*	PO//PO	0–0.1//2–6	
	PY-CLAY	PY-CLAY //PY-CLAY	0.1–0.3//1–4	
	SPHAL	SPHAL//SPHAL SPHAL//SPHAL/GAR	0.5–3//5–50 ?//> 50/40 – >100	
	GAR	SPHAL//SPHAL/GAR	?//> 50/40 – >100	Most common occurrence of GAR is in K-feldspar sites
	RHOD	RHOD//RHOD	0.5–5//0–2	

[1] See Table 1 for list of abbreviations and definitions of assemblages; an asterisk (*) next to an assemblage denotes a member of the suite of assemblages on the flanks of the Seriate center, and the remaining assemblages are members of the suite of assemblages above intrusive centers

[2] In this notation, two slashes separate assemblage comprising vein filling from assemblage comprising alteration envelope, and one slash separates assemblages comprising different mineralogic zones of a zoned envelope; detailed descriptions and measurements of individual veins, with relative proportions of each mineral in each zone, are in appendix B of Seedorff (1987)

[3] The notation used for vein types (see footnote 2) is used for the widths of zones, except that the names of mineral assemblages are replaced by the typical widths of the corresponding zones; the width of a vein filling is measured wall to wall; a fracture with negligible width is represented by a vein filling with a width of zero; the width of a zone in an envelope is the average width of the zones that are developed on both sides of the vein filling (i.e., the half-width of the total zone); a width of zero indicates that this zone is absent

A few, compositionally extraordinary hydrothermal micas, originally thought to be biotite, were later termed sericite and/or muscovite after electron microprobe analysis indicated that they are closer to being dioctahedral micas. All analyzed micas originally termed sericite or muscovite are dioctahedral.

As Gunow et al. (1980) and Munoz (1984) demonstrated, compositions of hydrothermal micas and garnets from Henderson are unusual, reflecting the fluorine-rich character of hydrothermal fluids and the highly differentiated, silicic compositions of mineralizing stocks and their wall rocks. The results reported here and discussed below tie mineral compositions to hydrothermal mineral assemblages and vein types, enlarge the analytical coverage to additional elements, and extend the known compositional ranges of these minerals (e.g., Gunow et al., 1980; van Middelaar and Keith, 1990).

FIG. 5. Simplified distribution and abundances of hydrothermal mineral assemblages by group. Each of the four panels shows members of one group of assemblages (see Table 1 for definitions and abbreviations of assemblages). In the high-temperature panel, each stock is outlined (compare to Fig. 2A) because intrusive contacts create prominent discontinuities in the distribution of high-temperature assemblages. In the other three panels, only the outlines of intrusive centers, Henderson (H), Seriate (S), and Vasquez (V), are shown.

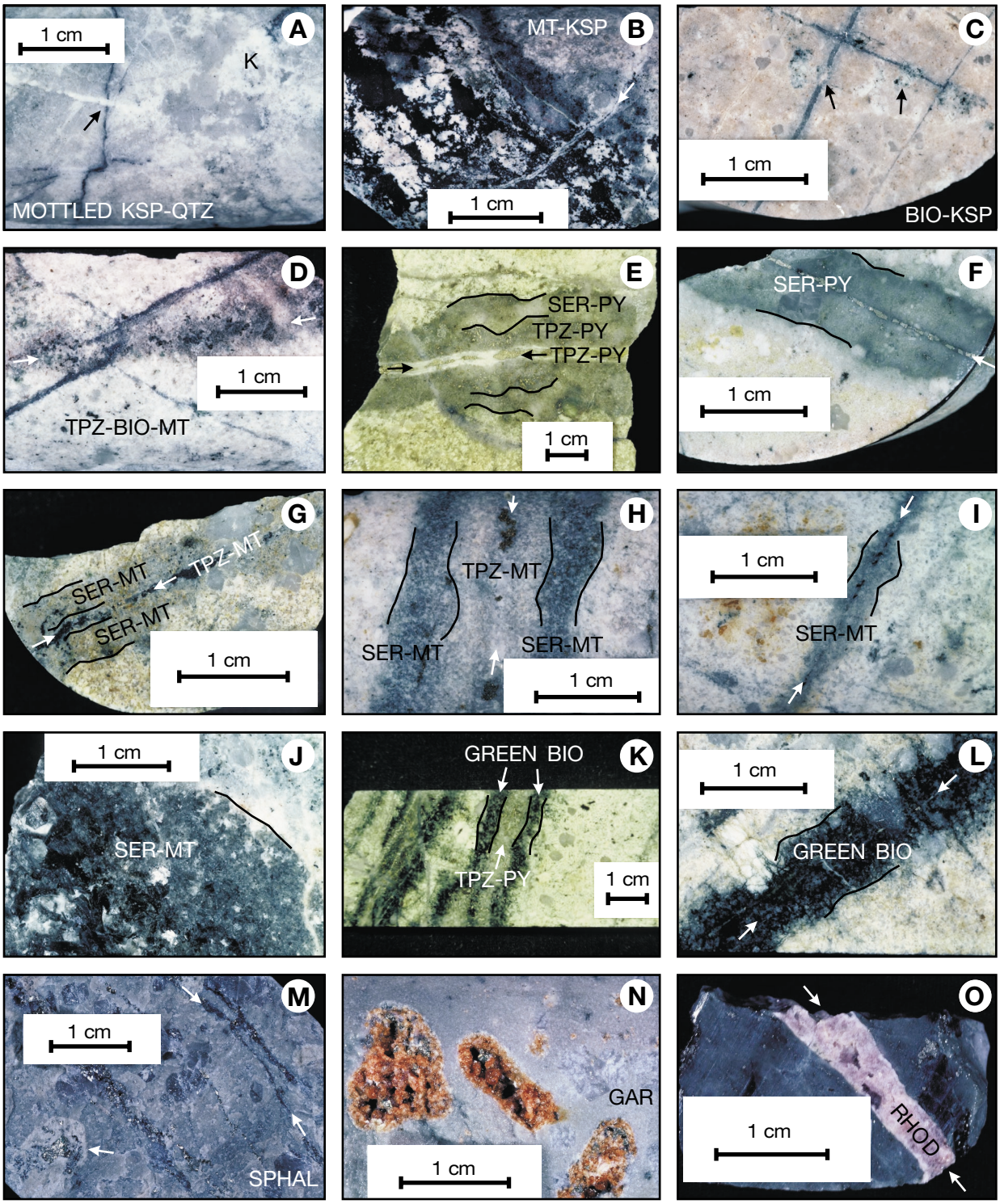

FIG. 6. Photographs of selected hydrothermal mineral assemblages and vein types. A. MOTTLED KSP-QTZ (sample H-321-314) illustrating destruction of primary texture, hairline K-feldspar veinlets cutting quartz-molybdenite vein of the QTZ-KSP-MO assemblage (black arrow pointing to intersection); K-feldspar phenocryst (black label K) in Urad porphyry is recrystallized to K-feldspar + quartz. B. MT-KSP (sample H-304-389) with unusually coarse-grained vein of magnetite + K-feldspar > fluorite + quartz cutting Urad porphyry, in turn cut by a magnetite veinlet with a K-feldspar envelope (white arrow), also a member of the MT-KSP assemblage. C. BIO-KSP (sample H-430-452.5) in Nystrom porphyry with veinlets of quartz + alkali feldspars + topaz + molybdenite and local brown biotite; the veinlets become quartz-poor and rich in topaz and alkali feldspars where transecting feldspar phenocrysts (black arrow on left). These veinlets have irregular envelopes of alkali feldspars + quartz > topaz + brown biotite + magnetite + ilmenorutile (several in photograph; one near right black arrow). D. TPZ-BIO-MT (sample H-497-1221.3) in Urad porphyry guided by an irregular fracture (aligned with white arrows), which cuts and offsets an earlier quartz-molybdenite vein of the QTZ-KSP-MO assemblage. E. Vein filling (aligned

Suite of assemblages above intrusive centers: In this suite, K-rich hydrothermal alkali feldspar developed in moderately high temperature assemblages; magnetite occurs with K-feldspar but not with sericite; topaz occurs almost entirely in a single, pyritic, feldspar-destructive assemblage; and a variety of pyrite-bearing assemblages formed at low temperatures (Table 1). Some assemblages form multiple zones of concentration (Table 7). Veins related to this suite of assemblages commonly have orientations similar to the radial set of high-temperature veins described by Carten et al. (1988b).

The moderately high temperature assemblage MOTTLED KSP-QTZ is characterized by aggregates of K-feldspar, quartz, minor fluorite, and rarely brown biotite (Table 1). The aggregates largely obliterate igneous texture and are laced with hairline veinlets of K-feldspar (Table 2). Where igneous textures are partially preserved, these veinlets appear to emanate from K-feldspar phenocrysts that were replaced by quartz and K-feldspar (Fig. 6A). Magmatic biotite and magnetite are destroyed. The MOTTLED KSP-QTZ assemblage forms a tabular zone above the Henderson and Seriate centers and is not found above the Vasquez center (Fig. 5B).

The magnetite ± K-feldspar ± quartz ± (molybdenite ± brown biotite ± topaz ± muscovite ± rutile) assemblage, symbolized by MT-KSP, consists largely of thin, irregular magnetite veinlets with narrow alteration envelopes of K-feldspar + magnetite + fluorite replacing magmatic feldspars (Tables 1–2; Fig. 6B). Magnetite was deposited preferentially where veinlets cut K-feldspar phenocrysts. The MT-KSP assemblage is concentrated in zones over both the Henderson and Seriate stocks and is found locally in and immediately above stocks of the Vasquez center (Fig. 5B). Uppermost occurrences of the assemblage extend well above the upper limit of the MOTTLED KSP-QTZ assemblage but coincide closely with uppermost occurrences of the QTZ-KSP-MO assemblage (Figs. 4–5A-B).

Most of the brown biotite in the MT-KSP assemblage was observed in a small region near the apex of the Seriate stock. The uncommon occurrences of this assemblage near the Vasquez stock, which are unusual for containing topaz and muscovite and could be regarded alternatively as a distinct assemblage, are associated with extraordinary mineral compositions: muscovite has very low Mg and very high Mn, Rb, and F contents; topaz is the most F rich of any analyzed from Henderson (Table 6). Seedorff (1988) also describes some minor, breccia-related occurrences of the MT-KSP assemblage.

The moderate-temperature assemblage TPZ-PY consists primarily of quartz, topaz, and pyrite, with minor fluorite and wolframite and rare hydrothermal garnet (Table 1). Core logging indicates that the TPZ-PY assemblage contains most of the wolframite in the deposit (Table 1); hence, this assemblage is the predominant host of tungsten at Henderson. Both rutile (in altered phenocrystic biotite and titanomagnetite sites) and ilmenorutile have been identified petrographically and by EDS analysis. Ilmenorutile was observed both as isolated grains and as intergrowths with wolframite. The TPZ-PY assemblage occurs in through-going veinlets and veins commonly with parallel walls, open-space fillings dominated by topaz and pyrite, and zoned alteration envelopes (Table 2; Fig. 6E). Pyrite commonly is found in the vein filling where

black arrows) and inner envelope of the TPZ-PY assemblage with an outer envelope of the SER-PY assemblage in Urad porphyry (sample H-33 7500 9H). Topaz is bright white; pyrite is brassy, quartz is gray. Beyond outer alteration front of the SER-PY assemblage, there is a clay alteration wash in which plagioclase was altered to clay minerals (brownish splotches) without sulfides, interpreted to have formed during a late alteration event superimposed on the entire sample. Note that an earlier quartz-molybdenite vein of the QTZ-KSP-MO assemblage is cut and offset by the TPZ-PY vein just to the right of the tip of the black arrow at left. F. SER-PY (sample H-378-690) in East Lobe porphyry with vein filling (white arrow) of pyrite > quartz + sericite with trace wolframite, with an alteration envelope of quartz + sericite > pyrite + rutile. Note that the clay alteration wash (golden brown patches of clay minerals without sulfides after plagioclase) developed beyond the greenish gray sericitic alteration front but is not formed in the whitish band within 0.2 mm of the edge of the sericitic envelope, reflecting a cryptic outer alteration zone. G. Magnetite-rich, alkali feldspar-bearing vein filling of the TPZ-MT assemblage (aligned white arrows) with an alteration envelope of the SER-MT assemblage hosted by Urad porphyry (sample H-508-357.7). Magnetite in the sericitic envelope is locally sulfidized to pyrite (related to partial superposition by younger events), and there is a clay alteration wash that is apparent in plagioclase phenocryst sites beyond the sericitic envelope. H. Irregular fracture (aligned white arrows) guides development of inner zone of the TPZ-MT assemblage and an outer envelope of the SER-MT assemblage (sample CX-158-2549) hosted by Urad porphyry. In both zones, magnetite is locally sulfidized to pyrite by younger events. I. Relatively magnetite-rich vein filling (aligned white arrows) of the SER-MT assemblage with an alteration envelope of the SER-MT assemblage hosted by Urad porphyry (sample H-323-616). J. Vein filling of white mica that is coarse grained enough to warrant the term muscovite (bladed, 0.2–1.1 mm) + albite + quartz >> magnetite of the SER-MT assemblage, with an envelope of the SER-MT assemblage, consisting of quartz + muscovite, grading to sericite toward the alteration front; even near the vein filling, replacement of magmatic feldspars by white mica is incomplete. Seriate porphyry hosts the vein (sample H-488-697.4). K. Several examples of inner envelopes of the TPZ-PY assemblage guided by irregular fractures that are bordered by outer envelopes of the GREEN BIO assemblage, hosted by Urad porphyry (sample H-323-842). Inner envelopes contain quartz + topaz + pyrite; outer envelopes contain green biotite + topaz > pyrite + sphalerite + fluorite + rutile. L. A narrow veinlet (aligned white arrows) of quartz > green biotite >> pyrite + topaz, with an envelope of green biotite > quartz >> pyrite, hosted by Urad porphyry (sample H-433-605.5). M. The SPHAL assemblage occurring here as sheeted veins (one shown by aligned white arrows) of pyrite >> sphalerite > quartz, but the assemblage persists as an alteration envelope extending into the host rock, Red Mountain border (sample CX-93-814). Note partial replacement of K-feldspar phenocryst near arrow at lower left. N. The GAR assemblage, with garnet + quartz + clay + pyrite >> sphalerite, with microscopic inclusions of chalcopyrite, hosted by Red Mountain border (sample CX-163-825). Most garnets occur as clusters of orange, euhedral grains filling K-feldspar phenocryst sites with other minerals of the assemblage, but garnet is also found in biotite phenocryst sites, with pyrite + rutile. O. Vein of banded, growth-zoned rhodochrosite > fluorite > clay + pyrite of the RHOD assemblage, cutting the Red Mountain porphyry, which had previously been sericitically altered (sample CX-103-2363).

TABLE 3. Representative Electron Microprobe Analyses of Feldspar

Sample no.[1]		H-321-314-[2]	CX-112-2439-[1]	H-430-452.5-[2](2)	H-488-713.9-[1](5)	H-430-452.5-[1](2)	H-499-292.3-[1](3)	H-499-292.3-[2](3)	CX-98-2908-[2]	H-488-697.4B-[1]
Mineral assemblage[2]		MOTTLED KSP-QTZ[3]	MT-KSP[4]	BIO-KSP*[5]	BIO-KSP*[6]	BIO-KSP*[7]	TPZ-BIO-MT*[8]	TPZ-BIO-MT*[9]	TPZ-MT*[10]	SER-MT*[11]
Site (number of spots per analysis)[12]		Recrystallized K-feldspar phenocryst (5)	Vein filling (5)	Vein filling (1)	Vein filling (1)	Envelope, replacing plagioclase phenocryst (1)	Vein filling (1)	Envelope, replacing groundmass feldspar (1)	Vein filling (5)	Envelope, replacing K-feldspar phenocryst (6)
SiO_2		65.45	65.21	65.92	68.58	64.80	65.44	68.87	65.71	67.05
Al_2O_3		18.55	18.54	18.63	20.01	18.46	18.55	19.46	18.54	20.44
Fe_2O_3*		0.01	0.30	0.08	0.04	0.20	0.08	0.04	0.02	0.12
TiO_2		0.01	0.01	NA	0.07	NA	NA	NA	0.01	0.01
CaO		0.04	0.01	0.13	0.46	0.10	0.03	0.13	0.00	0.62
K_2O		14.80	15.12	11.50	0.27	13.86	14.02	0.28	13.98	0.40
Na_2O		1.54	1.11	3.89	11.56	2.11	1.91	11.71	2.08	11.31
Rb_2O		0.08	0.10	0.11	0.00	0.15	0.09	0.00	0.14	0.01
Total[13]		100.48	100.40	100.26	100.99	99.68	100.12	100.49	100.48	99.96
					Number of moles on basis of $\Sigma IV = 4$					
IV	Si	3.00	2.99	3.00	2.97	2.99	3.00	3.00	3.00	2.94
	Al	1.00	1.00	1.00	1.02	1.00	1.00	1.00	1.00	1.06
	Fe	0.00	0.01	0.00	0.00	0.01	0.00	0.00	0.00	0.00
	Ti	0.00	0.00	—	0.00	—	—	—	0.00	0.00
	ΣIV	4.00	4.00	4.00	4.00	4.00	4.00	4.00	4.00	4.00
A	Na	0.14	0.10	0.34	0.97	0.19	0.17	0.99	0.18	0.96
	Ca	0.00	0.00	0.01	0.02	0.00	0.00	0.01	0.00	0.03
	K	0.86	0.88	0.67	0.01	0.82	0.82	0.02	0.81	0.02
	Rb	0.00	0.00	0.00	0.00	0.00	0.00	0.00	0.00	0.00
	ΣA	1.01	0.99	1.02	1.01	1.01	0.99	1.01	1.00	1.01
					Mole %					
X_{Or}		86	90	66	01	81	83	02	82	02
X_{Ab}		14	10	34	96	19	17	98	18	95
X_{An}		00	00	01	02	00	00	01	00	03

Analyses by E. Seedorff; oxides are reported in wt percent; N.A. = not analyzed; Fe_2O_3* = total Fe as Fe_2O_3; — = does not apply; site occupancy totals may vary ±0.01 due to rounding

[1] Notation for sample numbers: letters for drill hole series-number of drill hole in series-footage from collar of hole-[grain number](point number, only for inhomogeneous grains)

[2] See Table 1 for list of abbreviations; an asterisk (*) next to an assemblage denotes a member of the suite of assemblages on the flanks of the Seriate center, and the remaining assemblages are members of the suite of assemblages above intrusive centers; descriptions of samples tied to superscripts use the following notation: minerals in vein filling (width)//minerals in inner alteration envelope (half width)/minerals in outer alteration envelope (half width); analyzed mineral is italicized; minerals in parentheses are present in minor quantities

[3] Intergrown quartz + *K-feldspar*, associated with hairline K-feldspar veinlets (<0.1–0.3 mm) in totally recrystallized Urad porphyry

[4] Magnetite > *K-feldspar* > quartz + fluorite, massive vein (>2 cm); hosted by Urad porphyry

[5] Quartz >> molybdenite + (*alkali feldspar* + topaz) (0.1 mm)//alkali feldspar + (topaz + biotite + magnetite) (<0.1 mm); hosted by Nystrom porphyry

[6] Quartz + molybdenite > *alkali feldspar* + brown biotite > topaz + magnetite + rare earth oxide mineral + fluorite (2 – 3 mm)//quartz + alkali feldspar + brown biotite > topaz + molybdenite + magnetite + (fluorite), with trace sericite halos around molybdenite where adjacent to K-feldspar (6–8 mm); hosted by rhyolite porphyry dike that cuts Seriate porphyry

[7] Quartz >> molybdenite + (alkali feldspar + topaz) (0.1 mm)//*alkali feldspar* + (topaz + brown biotite + magnetite), with latter three minerals replacing cores of plagioclase phenocryst sites [(rims stable] (<0.1 mm); hosted by Nystrom porphyry

[8] (*Alkali feldspar* + topaz) (negligible width)//alkali feldspar > brown biotite + quartz > topaz > (magnetite + ilmenorutile) (2–3 mm); hosted by Urad porphyry

[9] (Alkali feldspar + topaz) (negligible width)//*alkali feldspar* > brown biotite + quartz > topaz > (magnetite + ilmenorutile) (2–3 mm); hosted by Urad porphyry

[10] Magnetite + *K-feldspar* + topaz + (quartz) (0.5–2 mm)//quartz + sericite >> magnetite (0.5–2 mm); hosted by Seriate Intermediate

[11] Muscovite (coarse grained, 0.2–1.1 mm, bladed) + *albite* + quartz >> magnetite (15 mm)//quartz + muscovite [coarse grained] grading to sericite [fine grained] toward alteration front + magnetite (25 mm); hosted by Seriate porphyry

[12] Number of spots per reported analysis, which is 1 only for compositionally inhomogeneous grains

[13] Searched for Mg, Pb, F, Sr, Ba, and Cs, but all were at or below detection

feldspar phenocrysts are transected. An inner envelope of this assemblage commonly is present, which tends to have high quartz content—particularly at the outer edge of the envelope—with lesser topaz and pyrite. The most common outer envelope is the SER-PY assemblage (Fig. 6E; described below). In a region about the Seriate center, the vein envelope instead consists of a GREEN BIO assemblage (quartz + green biotite ± topaz ± fluorite ± pyrite [or magnetite instead of pyrite] ± sphalerite ± garnet ± (sericite ± rutile ± ilmenorutile); Fig. 6K; described below). The TPZ-PY assemblage exhibits two partially overlapping zones of concentration over the Henderson and Seriate centers (Fig. 5C). The upper limit of this

assemblage is no higher than the upper extent of the QTZ-KSP-MO and MT-KSP assemblages (Figs. 4–5).

Electron microprobe analyses of garnet in the TPZ-PY assemblage (Table 5), which is rare in the assemblage, indicate that these garnets are Sn bearing and are the most Mn and F rich of any analyzed from Henderson (Table 6). In a reconnaissance survey of wolframite compositions, all grains analyzed by electron microprobe exhibited variable Fe and Mn contents, which is common for wolframite (Shawe et al., 1984; Campbell and Petersen, 1988). Individual spot analyses have molar Fe/(Fe + Mn) ratios that range from 0.51 to 0.73—in other words, richer in the ferberite end member of the solid-solution series than huebnerite (Table 5). Nonetheless, wolframite from Henderson—and other Climax-type deposits—previously had been referred to as huebnerite (e.g., Wallace et al., 1968, p. 626; 1978, p. 357; White et al., 1981, p. 304).

The assemblage SER-PY consists of quartz, sericite, pyrite, minor rutile and fluorite, and rare garnet and wolframite (Table 1). The volumetrically most important vein type containing this assemblage consists of pyrite-rich veinlets with greenish gray to lime green alteration envelopes of the assemblage that abuts K-feldspar–stable wall rocks (Fig. 6F). This type of vein is similar to the sericitic veinlets in porphyry copper deposits. In regions where TPZ-PY is the most abundant assemblage, near the apices of the Henderson and Seriate stocks (Fig. 5C), the SER-PY assemblage also occurs as envelopes fringing veins ± inner alteration envelopes of the TPZ-PY assemblage (Table 2; Fig. 6E). This second habit of the SER-PY assemblage contributes as much as half of the total volume of the assemblage in any interval of core in that region; elsewhere in the deposit, its contribution is greatly subordinate to the first habit. Although the SER-PY assemblage extends in trace abundances downward nearly into the Vasquez center, it is most abundant in two zones of concentration above the Henderson and Seriate centers, with the one over the Henderson center located at higher elevations than the one above Seriate (Fig. 5C). The distributions of the SER-PY and TPZ-PY assemblages overlap considerably, but the upper limits of formation and the zones of highest concentration of the SER-PY assemblage are slightly higher than for the TPZ-PY assemblage (Fig. 5C).

The low-temperature assemblage PY-CLAY is characterized by pyritic veinlets with envelopes of clay that commonly contain relict magmatic K-feldspar and locally contain carbonate. Short-wave infrared spectrometer analyses suggest that the clay minerals are sericite + illite ± kaolinite mixtures. This assemblage is most abundant over the Henderson and Seriate centers, especially above and lateral to the areas where the SER-PY assemblage is the most intense, and in a weakly developed zone above the Vasquez center (Fig. 5D). Garnet locally joins the assemblage at moderate to deep levels in the deposit.

The SPHAL assemblage occurs sparsely throughout the deposit but forms three distinct zones of concentration (Fig. 5D). This assemblage consists of base metal veins with abundant pyrite, sphalerite with chalcopyrite blebs, and lesser galena; these same sulfides occur as disseminations in the wall rock adjacent to some of the veins (Tables 1–2; Fig. 6M). At high levels in the deposit, inner envelopes of the SPHAL assemblage are fringed by outer envelopes of the GAR assemblage.

The GAR assemblage contains the vast majority of garnet in the system (Table 1); aside from Seedorff (1987, 1988), previous references to hydrothermal garnet at Henderson (e.g., Ranta et al., 1976; Gunow et al., 1980; White et al., 1981) generally refer only to this assemblage. Nonetheless, garnet is a minor component of many other assemblages (Table 1), especially around the Seriate center. The distribution of the GAR assemblage is largely restricted to high levels in the system, seemingly forming a single zone of concentration related to the Henderson center (Fig. 5D). In the GAR assemblage, garnet was deposited with sulfides as clusters of subhedral to euhedral grains, some of which appear to have grown in open space. Garnet occurs mostly in altered K-feldspar phenocryst sites (Fig. 6N), less commonly in other phenocrysts and groundmass feldspar grains, and rarely as isolated veins. Although the GAR assemblage has the appearance of being a product of pervasive replacement at the hand-specimen scale, it is described by Seedorff (1988) as constituting broad outer envelopes fringing inner envelopes and veins of the SPHAL assemblage (Table 2).

All garnets from the GAR assemblage analyzed with the electron microprobe (Tables 5–6) are compositionally homogeneous grains, in spite of optical growth zoning. Smyth et al. (1990) refined the crystal structure of a hydrothermal garnet from this assemblage at Henderson and determined that fluorine substitutes for oxygen in Si-absent tetrahedra in the garnet structure.

The final low-temperature assemblage is RHOD (Table 1). The key mineral in this assemblage is a pink carbonate mineral whose composition has not been determined; we follow historical precedent (e.g., Ranta et al., 1976) in referring to it as rhodochrosite. The RHOD assemblage is widely distributed (Fig. 5D), mainly as veinlets that cut all other veins in the Henderson system (Fig. 6O), but it also locally coats vugs containing garnet of the GAR assemblage.

White clay minerals that swell and turn yellow or tan in color after several months of exposure to air are developed to varying degrees throughout the deposit (Seedorff, 1988, p. 383), ranging from dusting of plagioclase phenocrysts to complete, direct replacement of both plagioclase and K-feldspar phenocrysts. In contrast to other low-temperature assemblages (including PY-CLAY), these clay minerals are not obviously related to veinlets and were not deposited with iron sulfides. This type of clay alteration was not studied in detail but is best developed in the Vasquez center deep in the deposit in rocks that are otherwise relatively unaltered, such as in the lower argillic zone of MacKenzie (1970) and White et al. (1981). These clay minerals may be of hydrothermal origin, perhaps forming at very low temperatures and late, following deposition of the RHOD assemblage. X-ray diffraction determinations by MacKenzie (1970) and short-wave infrared spectrometer analyses of representative samples indicate that the predominant clay minerals are kaolinite and montmorillonite.

Suite of assemblages on flanks of the Seriate center: Compared to the first suite, this suite of six assemblages (Table 1, asterisks) is distinguished by widespread and locally abundant hydrothermal biotite, widespread topaz, alkali feldspars of K-rich, K-Na, and Na-rich compositions, abundant magnetite, and local pyrrhotite. These six assemblages are collectively equivalent to the greisen zone of previous workers—a

TABLE 4. Representative Electron Microprobe Analyses of Biotite and White Mica

Sample no.[1]		H-129-465B-[1]	H-353-504-[1]	H-488-1037.1-[2]	H-430-452.5-[1]	H-499-460.2-[1]	80-401-[1]	H-323-842-[2]	CX-99-1669-[1]	H-488-697.4B-[1]
Mineral assemblage[2]		MOTTTLED KSP-QTZ[3]	MT-KSP[4]	MT-KSP[5]	BIO-KSP*[6]	TPZ-BIO-MT*[7]	GREEN BIO*[8]	GREEN BIO*[9]	SER-PY[10]	SER-MT*[11]
Site (number of spots per analysis)[12]		Clot in recrystallized mass (5)	Envelope (5)	Vein filling (5)	Envelope, replacing plagioclase phenocryst (5)	Envelope, possibly in a K-feldspar phenocryst site (5)	Envelope, at alteration front (5)	Outer envelope beyond inner envelope of TPZ-PY (5)	Outer envelope beyond inner envelope of TPZ-PY (5)	Envelope, replacing K-feldspar phenocryst (5)
Mineral		Brown biotite	Brown biotite	Muscovite	Brown biotite	Brown biotite	Sericite	Green biotite	Sericite	Muscovite
SiO_2		36.99	36.27	45.39	36.47	38.17	45.66	35.40	46.93	45.73
Al_2O_3		16.06	19.41	22.26	14.53	17.94	29.89	20.43	34.77	31.72
FeO* [13]		17.96	17.10	7.50	18.92	15.21	6.81	21.95	1.94	5.11
Fe_2O_3* [13]		2.24	2.08	0.92	2.34	1.90	0.00	2.70	0.24	0.63
TiO_2		1.29	1.45	0.04	1.56	1.31	0.19	0.33	0.21	0.28
MnO		0.80	0.89	7.23	2.58	0.93	0.53	5.95	0.05	0.38
MgO		11.06	8.35	0.01	10.62	9.66	1.46	0.07	0.64	0.41
ZnO		0.05	0.04	0.08	0.07	0.03	0.05	0.11	0.02	0.01
K_2O		9.06	9.43	10.03	9.25	9.14	10.59	9.30	10.18	10.33
Na_2O		0.31	0.32	0.04	0.33	0.30	0.42	0.07	0.62	0.54
CaO		0.11	0.02	0.00	0.10	0.08	0.00	0.06	0.06	0.02
F		5.93	4.06	8.00	5.26	5.20	3.02	3.57	2.34	3.04
Cl		0.13	0.15	0.01	0.11	0.09	0.01	0.06	0.01	0.01
BaO		0.01	0.02	0.00	0.03	0.02	0.00	0.02	0.02	0.01
Rb_2O		0.22	0.28	0.78	0.54	0.37	0.37	0.56	0.09	0.26
Subtotal[14]		102.21	99.87	102.29	102.70	100.35	99.00	100.58	98.11	98.48
O = (F + Cl)		–2.53	–1.74	–3.37	–2.24	–2.21	–1.27	–1.52	–0.99	–1.28
H_2O*		1.09	1.98	0.30	1.38	1.48	2.93	2.09	3.40	2.95
Total		100.80	100.12	99.22	101.87	99.64	100.66	101.18	100.53	100.15
		Number of moles on basis of Σ *IV* + *VI* cations is >6 and <7[13]								
IV	Si	2.82	2.76	3.33	2.80	2.88	3.14	2.80	3.12	3.13
	Al^{IV}	1.18	1.24	0.67	1.20	1.12	0.86	1.20	0.88	0.87
	Σ *IV*	4.00	4.00	4.00	4.00	4.00	4.00	4.00	4.00	4.00
VI	Al^{VI}	0.26	0.50	1.25	0.12	0.48	1.56	0.70	1.84	1.68
	Ti	0.07	0.08	0.00	0.09	0.07	0.01	0.02	0.01	0.01
	Fe^{3+}	0.13	0.12	0.05	0.13	0.11	0.00	0.16	0.01	0.03
	Fe^{2+}	1.14	1.08	0.46	1.21	0.96	0.39	1.44	0.11	0.29
	Mn	0.05	0.06	0.45	0.17	0.06	0.03	0.40	0.00	0.02
	Mg	1.26	0.95	0.00	1.22	1.09	0.15	0.01	0.06	0.04
	Zn	0.00	0.00	0.00	0.00	0.00	0.00	0.01	0.00	0.00
	Σ *VI*	2.91	2.79	2.21	2.94	2.77	2.14	2.74	2.03	2.07
A	Ca	0.01	0.00	0.00	0.01	0.01	0.00	0.01	0.00	0.00
	K	0.88	0.92	0.94	0.91	0.88	0.93	0.94	0.86	0.90
	Na	0.05	0.05	0.01	0.05	0.04	0.06	0.01	0.08	0.07
	Ba	0.00	0.00	0.00	0.00	0.00	0.00	0.00	0.00	0.00
	Rb	0.01	0.01	0.04	0.03	0.02	0.02	0.03	0.00	0.01
	Σ *A*	0.95	0.98	0.99	1.00	0.95	1.01	0.99	0.94	0.98
	F	1.43	0.98	1.85	1.28	1.24	0.66	0.89	0.49	0.66
	Cl	0.02	0.02	0.00	0.01	0.01	0.00	0.01	0.00	0.00
	OH*	0.56	1.01	0.15	0.72	0.75	1.34	1.11	1.51	1.34
X_{Mg}[15]		0.45	0.36	0.00	0.44	0.41	0.07	0.00	0.03	0.02

terminology that we do not use, for reasons discussed by Seedorff (1988, p. 389–391). In certain appropriately oriented drill holes, it can be shown that assemblages of this suite form sheeted vein sets subparallel to the moderately outward dipping, concentric set of high-temperature veinlets related to the Seriate center. After development of the PO assemblage (described below), this suite of assemblages on the flanks of the Seriate center merged with the suite best developed above intrusive centers.

The moderately high temperature assemblage BIO-KSP (Fig. 5B) is characterized by veinlets with envelopes in which feldspar phenocrysts are replaced by aggregates of alkali

TABLE 4. *(Cont.)*

Analyses by E. Seedorff; oxides are reported in wt percent; N.A. = not analyzed; — = does not apply; FeO* and Fe_2O_3* are calculated based on assumption of $Fe^{III}/(Fe^{II} + Fe^{III}) = 0.1$ (see footnote 13); H_2O* is a calculated value; site occupancy totals may vary ±0.01 due to rounding

[1] Key to sample numbers: letters for drill hole series-drill hole number-footage from collar of hole-[grain number]

[2] See Table 1 for list of abbreviations; an asterisk (*) next to an assemblage denotes a member of the suite of assemblages on the flanks of the Seriate center, and the remaining assemblages are members of the suite of assemblages above intrusive centers; see Table 3 for notation used in sample descriptions

[3] Intergrown K-feldspar + quartz > *brown biotite* (clots 0.1–0.3 mm, with individual grains <0.01 mm), associated with hairline veinlets of K-feldspar + brown biotite (<0.1–0.3 mm) in totally recrystallized Urad porphyry

[4] K-feldspar > brown biotite + magnetite [later mostly sulfidized to pyrite] > (topaz + quartz) (0.2–0.6 mm) associated with hairline K-feldspar veinlets//quartz + K-feldspar + *brown biotite* + magnetite > (topaz) (1–5 mm); hosted by Urad porphyry

[5] Quartz > magnetite >> fluorite + topaz + *muscovite* > (K-feldspar) (1.4–1.5 cm)//magnetite (disseminated; 0–1.5 cm); hosted by granite porphyry dike in Vasquez porphyry

[6] Quartz >> molybdenite+ (alkali feldspar + topaz) (0.1 mm)//alkali feldspar + (topaz + *brown biotite* + magnetite), with latter three minerals replacing cores of plagioclase phenocryst sites (rims stable) (<0.1 mm); hosted by Nystrom porphyry

[7] Fracture (negligible width)//quartz > alkali feldspar + *brown biotite* > fluorite > (topaz + magnetite [later locally sulfidized to pyrite] + ilmenorutile + wolframite) (1.5–3.0 mm); hosted by Urad porphyry

[8] Fracture (negligible width)//quartz + topaz + *sericite* [dark green in hand specimen, pleochroic reddish brown to brown in thin section] + garnet [encloses/rims sphalerite] + sphalerite [with local alteration to pyrrhotite from a superimposed event] > pyrite > (rutile [confirmed by EDS, in biotite sites] + ilmenorutile [confirmed by EDS]) (3–6 mm); abundance of sericite increases relative to topaz toward the alteration front; hosted by Henderson border with granitic-textured clots

[9] (Quartz + topaz + pyrite) (negligible width)//pyrite + quartz + topaz (7–10 mm)/*green biotite* + topaz > pyrite + sphalerite + fluorite + rutile (5–7 mm); abundances of topaz and pyrite increase toward inner envelope and abundances of sphalerite and fluorite increase toward alteration front; hosted by Urad porphyry

[10] Topaz >> quartz + pyrite >> (ilmenorutile) [confirmed by EDS] (1.0–1.5 mm)//quartz >> topaz + pyrite (0.2–0.5 mm)/quartz + *sericite* [grain size <0.01–0.1 mm, mostly <0.02 mm] + pyrite > fluorite > (rutile) [in biotite phenocryst sites] (2 cm); hosted by Urad porphyry

[11] *Muscovite* (coarse grained, 0.2–1.1 mm, bladed) + albite + quartz >> magnetite (15 mm)//quartz + muscovite [coarse grained] grading to sericite [fine grained] toward alteration front + magnetite (25 mm); hosted by Seriate porphyry

[12] Number of spots per reported analysis, which is 1 only for compositionally inhomogeneous grains

[13] Assume hydroxyl site is filled with OH, F, or Cl; optimized to charge balance = 0 and $Fe^{III}/(Fe^{II} + Fe^{III}) = 0.1$

[14] Searched for Cs but was at or below detection

[15] X_{Mg} = mole fraction magnesium, $X_{Mg} = Mg/\Sigma VI$ cations, equivalent to $X_{phlogopite}$ for biotite and $X_{celadonite}$ for sericite/muscovite

feldspars, quartz, brown biotite, and lesser topaz. Most commonly, these envelopes are related to veinlets that resemble veinlets associated with the QTZ-KSP-MO assemblage, except that molybdenite is less abundant and magnetite and other phases are present (Table 1). Where a veinlet cuts a feldspar phenocryst, however, the veinlet is quartz poor and dominated by alkali feldspars and brown biotite (Fig. 6C).

Backscattered electron images of the BIO-KSP assemblage reveal compositional domains of hydrothermal alkali feldspar that are irregularly intergrown on scales of 2 to 35 μm. K-rich, K-Na, and Na-rich compositions have been analyzed (Tables 1, 3, 6). As is the case for other assemblages, K-rich alkali feldspar is Rb bearing, whereas Na-rich alkali feldspar is Rb poor (Table 3).

The TPZ-BIO-MT assemblage (Table 1; Fig. 5B) differs from the BIO-KSP assemblage in that it only rarely contains molybdenite and has proportionately more brown biotite, magnetite, and topaz, and rarely contains garnet. Moreover, the TPZ-BIO-MT assemblage generally is related to irregular fractures of negligible width (Fig. 6D), and the texture and mineralogy of the alteration envelopes are not strongly controlled by intersections with phenocrysts. In common with the BIO-KSP assemblage, the TPZ-BIO-MT assemblage also appears to have alkali feldspars of three compositional ranges (Tables 1, 3, 6).

The TPZ-MT assemblage was the first moderate-temperature assemblage to form on the flanks of the Seriate center (Fig. 5C). In the most common type of vein (Table 2), this assemblage is fringed by a sericitic assemblage, SER-MT (Fig. 6G-H; described below); in this respect, the TPZ-MT assemblage is similar to the TPZ-PY assemblage of the suite of assemblages above intrusive centers. In contrast to TPZ-PY, there is another type of TPZ-MT vein that has fresh wall rocks without an intervening zone of the SER-MT assemblage. In some cases those veins contain K-feldspar in equilibrium with topaz.

The SER-MT assemblage (Fig. 5C), analogous to SER-PY, occurs in two principal vein types (Table 2): as outer envelopes fringing the TPZ-MT assemblage (Fig. 6G-H) and as envelopes bordering magnetite-bearing fractures (Fig. 6I). White mica in the SER-MT assemblage is distinct, however, in that in certain cases it attains a relatively coarse grain size (Fig. 6J); in those cases, it warrants the term muscovite (Seedorff, 1988, p. 389–391, discusses the term greisen; see also Shaver, 1991, p. 320–321).

The compositions of sericite and muscovite from the SER-MT assemblage are similar to one another and to sericite from the SER-PY assemblage (Tables 4, 6). Alkali feldspar that rarely accompanies muscovite is albitic in composition (Table 3).

GREEN BIO is a volumetrically minor assemblage that is of mineralogic and geochemical interest. This assemblage is generally restricted to the flanks of the Seriate center (Table 1), but it borders regions in the Seriate center where assemblages of the other suite are abundant (Fig. 5C) and exhibits characteristics of both suites. Technically, it is actually two uncommon assemblages, as both magnetite- and pyrite-bearing varieties of the GREEN BIO assemblage are present (note that magnetite and pyrite are shown as mutually incompatible phases in Table 1). The pyrite-bearing variety is regarded as being younger based on a single crosscutting relationship. Both varieties occur as envelopes adjacent to hairline fractures (Fig. 6L), but the pyrite-bearing variety also forms the outer envelope of zoned envelopes fringing the TPZ-PY

TABLE 5. Representative Electron Microprobe Analyses of Topaz, Wolframite, and Garnet

Sample no.[1]	H-074-24-[3]	H-499-295.2-[2]	H-499-292.3-[1]	H-049-166-[3](3)	H-471-255-[1]	H-519-239.6-[1](4)	CX-163-499-[1]	80-401-[2]
Mineral assemblage[2]	TPZ-PY[3]	BIO-KSP*[4]	TPZ-BIO-MT*[5]	TPZ-PY[6]	TPZ-PY[7]	SER-PY[8]	GAR[9]	GREEN BIO*[10]
Site (number of spots per analysis)[11]	Inner envelope, inside outer envelope of SER-PY (5)	Vein filling (5)	Vein filling (6)	Vein filling, inside inner envelope of TPZ-PY and outer envelope of SER-PY (1)	Vein filling, bordered by envelope of GREEN BIO (6)	Envelope bordering SER-PY, replacing groundmass feldspar (1)	Envelope?, in K-feldspar phenocryst site (5)	Envelope, at alteration front (8)
Mineral	Topaz			Wolframite	Garnet			
SiO_2	32.47	32.68	32.38	NA	30.37	33.55	33.85	34.81
TiO_2	0.01	0.01	NA	NA	0.03	0.08	0.07	0.05
SnO_2	NA	NA	NA	NA	0.15	0.00	0.04	0.03
Al_2O_3	55.18	55.24	55.32	NA	21.76	21.39	21.14	21.59
Fe_2O_3*	0.01	0.04	0.01	—	0.00	0.00	0.41	0.00
FeO*	—	—	—	17.04	2.38	5.54	3.20	7.14
Y_2O_3	NA	NA	NA	NA	0.00	0.00	0.52	0.00
WO_3	NA	NA	NA	76.63	NA	NA	NA	NA
MnO	NA	NA	NA	6.60	40.86	37.44	36.65	36.20
MgO	0.00	0.00	NA	NA	0.00	0.05	0.01	0.01
CaO	0.01	0.00	0.01	0.04	0.39	0.37	2.77	0.45
ZnO	NA	NA	NA	0.03	0.02	0.02	0.05	0.01
F	16.82	18.60	19.14	NA	5.59	3.49	2.56	2.06
Subtotal[12]	104.50	106.57	106.86	100.34	101.55	101.93	101.27	102.35
O = F	–7.08	–7.83	–8.06	—	–2.35	–1.47	–1.08	–0.87
H_2O*	1.77	0.96	0.69	—	—	—	—	—
Total	99.19	99.70	99.49	100.34	99.20	100.46	100.19	101.48
	Number of moles on basis of Σ *IV* + *VI* cations = 3			Basis of Σ cations = 2	Number of moles on basis of Σ cations <8[13]			
IV Si	1.00	1.00	0.99		*IV* Si	2.51	2.73	2.76	2.82
Al	0.00	0.00	0.01		Al	0.13	0.06	0.07	0.06
Σ *IV*	1.00	1.00	1.00		vac	0.36	0.21	0.17	0.12
					Σ *IV*	3.00	3.00	3.00	3.00
VI Al	2.00	2.00	2.00	*VI* W 1.00	*VI* Al	1.99	1.99	1.97	2.00
Fe^{3+}	0.00	0.00	0.00		Ti	0.00	0.00	0.00	0.00
Ti	0.00	0.00	—		Sn	0.00	0.00	0.00	0.00
Mg	0.00	0.00	—		Fe^{3+}	0.00	0.00	0.03	0.00
Ca	0.00	0.00	—		Σ VI	2.00	2.00	2.00	2.00
Cr	0.00	0.00	—						
Σ *VI*	2.00	2.00	2.00						
				M Fe^{2+} 0.72	*A* Mg	0.00	0.01	0.00	0.00
				Mn 0.28	Fe^{2+}	0.16	0.38	0.22	0.48
				Zn 0.00	Mn	2.86	2.58	2.54	2.48
				Ca 0.00	Ca	0.03	0.03	0.24	0.04
				Σ *M* 1.00	Y	0.00	0.00	0.02	0.00
					Zn	0.00	0.00	0.00	0.00
					Σ *A*	3.06	3.00	3.02	3.01
F	1.64	1.80	1.86		F	1.46	0.90	0.66	0.53
OH*	0.36	0.20	0.14						
$X_{F\text{-topaz}}$[14]	0.82	0.90	0.93	Fe/(Fe + Mn) = 0.72					

assemblage (Table 2; Fig. 6K)—a member of the other suite of assemblages. Both types of veins and both varieties of the assemblage commonly have sphalerite and may contain garnet, both of which tend to be most abundant toward the outer front of alteration envelopes. Fluorite, rutile, and ilmenorutile are minor or rare members of the assemblage.

Based on electron microprobe analyses, green biotites exhibit significant compositional variation between samples but

TABLE 5. *(Cont.)*

Notes: Analyses by E. Seedorff; oxides are reported in wt percent; N.A. = not analyzed; — = not present in this assemblage; FeO* = total Fe as FeO; Fe_2O_3* = total Fe as Fe_2O_3; all Fe in topaz assumed to be Fe^{III} and in wolframite assumed to be Fe^{II}; Fe^{III} and H_2O in garnet calculated based on charge balance and stoichiometry constraints; vac denotes tetrahedral site vacancy in fluorian garnet; analytical totals suggest no water present in garnet (assumed to be zero); H_2O* in topaz is a calculated value; site occupancy totals may vary ±0.01 due to rounding

[1] Key to sample numbers: letters for drill hole series-drill hole number-footage from collar of hole-[grain number](point number, only for inhomogeneous grains)

[2] See Table 1 for list of abbreviations; an asterisk (*) next to an assemblage denotes a member of the suite of assemblages on the flanks of the Seriate center, and the remaining assemblages are members of the suite of assemblages above intrusive centers; see Table 3 for notation used in sample descriptions

[3] Pyrite > topaz [grain size 0.05–5 mm] >> fluorite > (quartz) (4 mm)//quartz > *topaz* [grains <0.15 mm] > pyrite > fluorite (0.7 mm)/quartz + sericite [grains 0.03–0.1 mm] + pyrite + rutile (4 mm); hosted by Primos border

[4] Alkali feldspar + quartz + *topaz* + magnetite > (brown biotite + molybdenite) (>4 cm)//? [massive vein filling; envelope beyond edge of core]

[5] (Alkali feldspar + *topaz*) (negligible width)//alkali feldspar > brown biotite + quartz > topaz > (magnetite + ilmenorutile) (2–3 mm); hosted by Urad porphyry

[6] Pyrite + *wolframite* + fluorite (1.2 mm)//quartz >> topaz > (pyrite) (1 mm)/quartz + sericite > pyrite (>20 mm); hosted by Primos border

[7] Quartz + topaz + pyrite > *garnet* (4–5 mm)//quartz > topaz + green biotite + fluorite > garnet > (pyrite) (5–12 mm); hosted by Urad porphyry

[8] (Pyrite > quartz + sericite) (negligible width)//quartz + sericite [grain size <0.01–0.05 mm, mostly <0.02 mm] > pyrite > *garnet* + fluorite (15 mm); hosted by Urad porphyry

[9] (Uncertain)//clay > *garnet* + pyrite > sphalerite > galena (unknown width); hosted by Red Mountain border

[10] Fracture (negligible width)//quartz + topaz + green biotite [dark green in hand specimen, pleochroic reddish brown to brown in thin section] + *garnet* [encloses/rims sphalerite] + sphalerite [with local alteration to pyrrhotite from a superimposed event] > pyrite > (rutile [confirmed by EDS, in biotite sites] + ilmenorutile [confirmed by EDS]) (3–6 mm); abundance of green biotite increases relative to topaz toward the alteration front; hosted by Henderson border with granitic-textured clots

[11] Number of spots per reported analysis, which is 1 only for compositionally inhomogeneous grains

[12] Elements sought but not found: topaz: P, Cr; garnet: Cr, K, Na, Cl.

[13] Σ cations <8; optimized to charge balance = 0; optimized ideally to $F/IV_{vac} = 4$, checked against *IV* site occupancy = 3

[14] $X_{F\text{-topaz}}$ = mole fraction fluor-topaz in topaz solid solution, F/(F + OH*)

are typically aluminous and commonly manganiferous (Tables 4, 6). The siderophyllite-rich micas reported by Gunow et al. (1980) generally belong to the GREEN BIO assemblage.

PO is the only mineral assemblage at Henderson that contains pyrrhotite and the only low-temperature assemblage that is observed only on the flanks of the Seriate center. The PO assemblage has a highly restricted distribution (Fig. 5D) near occurrences of the GREEN BIO assemblage on the eastern side of the Seriate center, although in a less distal position. The PO assemblage is present where magnetite-bearing assemblages are most abundant and occurs as partial replacements of precursor magnetite; in turn, pyrrhotite subsequently was partially replaced by pyrite of still younger assemblages. Because of its restricted occurrence in an area of high geologic complexity, the assemblage is as yet poorly defined.

Correlation with standard alteration terminology

The specialized terminology for alteration-mineralization at Henderson is correlated with the terminology of alteration types in Figure 7. Alteration types loosely follow those of Meyer and Hemley (1967) and Barton et al. (1991) but are defined using a mineralogically based, chemical classification system that is based on cation to hydrogen ion activity ratios in the fluid (Seedorff, 1986, 1987, p. 158–163). Transitional types are defined as assemblages that share mineralogic characteristics with two or more types, as distinct from the Transitional stage of Gustafson and Hunt (1975) that is transitional in time between feldspar-stable and feldspar-destructive assemblages.

The high-temperature assemblages contain the only representative of silicic alteration and an intense potassic assemblage. Both suites of lower temperature assemblages contain examples of potassic, sericitic, and intermediate argillic types (or transitional counterparts). No assemblage is of the advanced argillic type (cf. Burt, 1981, p. 832). On the basis of occurrence of Na and intermediate K-Na feldspars, several assemblages from the suite that formed on the flanks of the Seriate center are transitional types of assemblages (or are locally transitional to another type), potassic-sodic, sericitic-potassic, and sericitic-sodic (Table 1; Fig. 7).

Topaz is absent in high-temperature assemblages. The only topaz-bearing assemblage in the suite formed above intrusive centers is of the sericitic type. Topaz is present in transitional potassic-sodic– and sericitic-sodic–type assemblages in the suite formed on the flanks of the Seriate center. The presence of topaz in potassic assemblages, though common in pegmatites, is unusual for hydrothermal ore deposits (Seedorff, 1986). In other porphyry-related deposits, topaz generally occurs in assemblages of the advanced argillic and sericitic types (Meyer and Hemley, 1967; Rose and Burt, 1979).

Although only a crude correlation can be made with Henderson, the terminology developed for the main porphyry copper deposit (Turquoise Gulch) in the Indio Muerto district at El Salvador, Chile (Gustafson and Hunt, 1975; Gustafson and Quiroga G., 1995) is a standard for comparing alteration-mineralization stages and vein types among porphyry systems. The analogy is imperfect, but the distinctive suite of assemblages on the flanks of the Seriate center at Henderson may have a rough counterpart at Turquoise Gulch in the distinctive assemblages and vein types developed at deeper levels (Gustafson and Quiroga G., 1995), compared to those formed at intermediate and shallow levels (Gustafson and Hunt, 1975). The high- and moderately high temperature assemblages at Henderson correspond roughly to the Early stage and A veinlets of El Salvador. There is no good analogue at Henderson for the Transitional stage and B veins, which contain practically all the Mo at the Turquoise Gulch deposit, although the moderate-temperature TPZ-PY assemblage is the best candidate at Henderson on the basis of relative age.

TABLE 6. Compositional Ranges of Selected Hydrothermal Minerals in Lower Temperature Mineral Assemblages[1]

Temperature group		Moderately high[2]				Moderate[2]					Low[2]	
Mineral	Compositional characteristic	MOTTLED KSP-QTZ	MT-KSP	BIO-KSP*	TPZ-BIO-MT*	TPZ-PY	SER-PY	TPZ-MT*	SER-MT*	GREEN BIO*	PY-CLAY	GAR
K-feldspar	X_{Or}	0.86–0.88	0.90	0.78–0.81	0.75–0.87	—	—	0.80–0.82	—	—	—	—
	X_{Ab}	0.12–0.14	0.10	0.19–0.22	0.13–0.25			0.18–0.20				
	X_{An}	0.00	0.00	0.00–0.01	0.00			0.00				
K-Na feldspar	X_{Or}	—	—	0.59–0.71	0.43–0.65	—	—	—	—	—	—	—
	X_{Ab}			0.29–0.40	0.35–0.56							
	X_{An}			0.00–0.01	0.00–0.04							
Na feldspar	X_{Or}	—	—	0.01–0.11	0.02–0.27	—	—	—	0.02	—	—	—
	X_{Ab}			0.86–0.96	0.71–0.98				0.95			
	X_{An}			0.02–0.08	0.01–0.02				0.03			
Biotite	X_{Mg}	0.33–0.45	0.36–0.37	0.17–0.47	0.11–0.41	—	—	—	—	0.02–0.05	—	—
	Mn (apfu)	0.05	0.05–0.06	0.06–0.17	0.06–0.27					0.10–0.40		
	Rb (apfu)	0.01	0.01	0.02–0.03	0.02–0.03					0.02–0.04		
	F (apfu)	0.97–1.42	0.97–1.21	0.79–1.34	0.99–1.24					0.50–1.47		
	Cl (apfu)	0.01	0.02	0.01	0.01–0.02					0.00–0.01		
Sericite/ Muscovite	X_{Mg}	—	0.00	—	—	—	0.01-0.07	—	0.02-0.03	0.07	—	—
	Mn (apfu)		0.25–0.45				0.00–0.02		0.01–0.02	0.03		
	Rb (apfu)		0.04				0.00–0.01		0.01	0.02		
	F (apfu)		1.27–1.85				0.44–0.60		0.55–0.66	0.66		
	Cl (apfu)		0.00				0.00		0.00	0.00		
Topaz	$X_{F\text{-}topaz}$	—	0.94–1.00	0.76–0.96	0.83–0.97	0.80–0.96	—	0.77–0.93	—	0.86	—	—
Garnet	Mn (apfu)	—	—	—	N.A.	2.86–2.88	2.45–2.58	2.37–2.41	2.45	2.48–2.51	N.A.	2.39–2.54
	Fe^{3+} (apfu)					0.00–0.01	0.00–0.02	0.00–0.01	0.00	0.00		0.02–0.08
	Fe^{2+} (apfu)					0.16	0.33–0.61	0.34–0.62	0.48	0.43–0.48		0.19–0.34
	Ca (apfu)					0.03	0.03–0.04	0.02	0.05	0.03–0.04		0.20–0.31
	F (apfu)					1.45–1.46	0.68–0.90	0.34–0.51	0.81	0.49–0.53		0.42–0.69

[1] Summarized in terms of mole fractions (X) of end-member compositions and atoms per formula unit (apfu) of an element in a given mineral; in feldspars, X_{Or} = K/(K + Na + Ca), X_{Ab} = Na/(K + Na + Ca), and X_{An} = Ca/(K + Na + Ca); in micas, X_{Mg} = mole fraction magnesium, equivalent to $X_{phlogopite}$ for biotite and $X_{celadonite}$ for sericite and/or muscovite, X_{Mg} = Mg/(total octahedral cations); $X_{F\text{-}topaz}$ = mole fraction fluor-topaz, F/(F + OH*); — = not present in this assemblage; NA = not analyzed from this assemblage

[2] See Table 1 for list of abbreviations and definitions of assemblages; an asterisk (*) next to an assemblage denotes a member of the suite of assemblages on the flanks of the Seriate center, and the remaining assemblages are members of the suite of assemblages above intrusive centers

TABLE 7. Comparison of Spatial Versus Temporal Characteristics of Assemblages

Group	Assemblage[1]	Interpretation of number of zones[2]	Preferred interpretation of number of events or cycles[2]
High temperature	QTZ-FL and QTZ-KSP-MO, undivided	1 associated with each mineralized stock (7 significant zones)	1 cycle associated with each stock (7 significant plus 5 minor cycles)
Moderately high temperature	MOTTLED KSP-QTZ	2 (1 each above Henderson and Seriate centers)	2 cycles
	MT-KSP	3 (1 above each intrusive center)	2 major plus 2 minor cycles
	BIO-KSP*	1 (on flanks of Seriate center)	1 event (beginning after Seriate ore zone formed)
	TPZ-BIO-MT*	1 (on flanks of Seriate center)	1 event (beginning after Seriate ore zone formed)
Moderate temperature	TPZ-PY	2 (1 each above Henderson and Seriate centers)	1 event (beginning after Seriate ore zone formed)
	SER-PY	2 (1 each above Henderson and Seriate centers)	1 event (beginning after Seriate ore zone formed)
	TPZ-MT*	1 (on flanks of Seriate center)	1 event (beginning after Seriate ore zone formed)
	SER-MT*	1 (on flanks of Seriate center)	1 event (beginning after Seriate ore zone formed)
	GREEN BIO*	1 (on flanks of Seriate center)	1 event (beginning after Seriate ore zone formed)
Low temperature	PO*	1 (on flanks of Seriate center)	1 event (probably beginning after Vasquez ore zone formed)
	PY-CLAY	3, although poorly defined (1 above each intrusive center)	1 event (probably beginning after Vasquez ore zone formed)
	SPHAL	3, exceptionally well defined (1 above each intrusive center)	1 event (probably beginning after Vasquez ore zone formed)
	GAR	1? (above Henderson center, although perhaps composite of Henderson and Seriate centers)	1 event (probably beginning after Vasquez ore zone formed)
	RHOD	3 (1 above each intrusive center)	1 event (probably beginning after Vasquez ore zone formed)

[1] See Table 1 for list of abbreviations and definitions of assemblages, except high-temperature assemblages, which are explained in text; an asterisk (*) next to an assemblage denotes a member of the suite of assemblages on the flanks of the Seriate center, and the remaining assemblages are members of the suite of assemblages above intrusive centers

[2] See Seedorff (1988) for a discussion of uncertainties in interpretation

The moderate- and low-temperature assemblages at Henderson correspond loosely to the Late stage at El Salvador, with veinlets of the SER-PY assemblage at Henderson (Fig. 6F) corresponding closely to the classic D veinlets of El Salvador.

Crosscutting Relationships

The relative ages of hydrothermal events are determined by direct observation of crosscutting relationships between veins and intrusions at intrusive contacts, and by crosscutting relationships between veins of various types at various spatial positions, which are interpreted in light of the three-dimensional distributions of mineral assemblages and vein types and the geometry and relative ages of intrusions. Photographs of key crosscutting relationships are shown in Figure 8, and observations are summarized in Figures 9 and 10.

Crosscutting relationships between intrusions and veins

The ability to capture key crosscutting relationships unambiguously at intrusive contacts of the various stocks is uneven, as it depends on the geologic preservation of contacts (some are engulfed by subsequent intrusions) and the degree to which the contacts of that stock are exposed by drilling and drifting. Drill holes logged along two cross sections for this study pierce intrusive contacts at many locations, as shown in figures 3 and 4 of Seedorff (1988). Carten et al. (1988b) did not show maps of all levels and workings, but their figures 1, 2 (inset), and 13 are illustrative of the numerous mapped drifts that cross intrusive contacts. Photographs of key relationships at intrusive contacts are shown in Carten et al. (1988b, fig. 6) and Figure 8G-H.

No veins of any kind, including those of the high-temperature assemblages, are cut off at the boundaries between the textural phases of stocks (e.g., transition from Seriate Border to Seriate Intermediate of Carten et al., 1988b). Where dikes that formed during crystallization of deeper and/or interior phases cut upward or outward through shallower and/or exterior phases, however, high-temperature veins are cut off at the dike contacts (Carten et al., 1988b, p. 292), but veins related to lower temperature assemblages are not cut off at such contacts where the dikes are within their source stock (e.g., a dike of Seriate Intermediate cutting Seriate Border).

At contacts between two stocks of the same intrusive center (e.g., Nystrom and Seriate stocks in the Seriate center, Figs. 2A, 3C), the only veins that are cut off are veins related

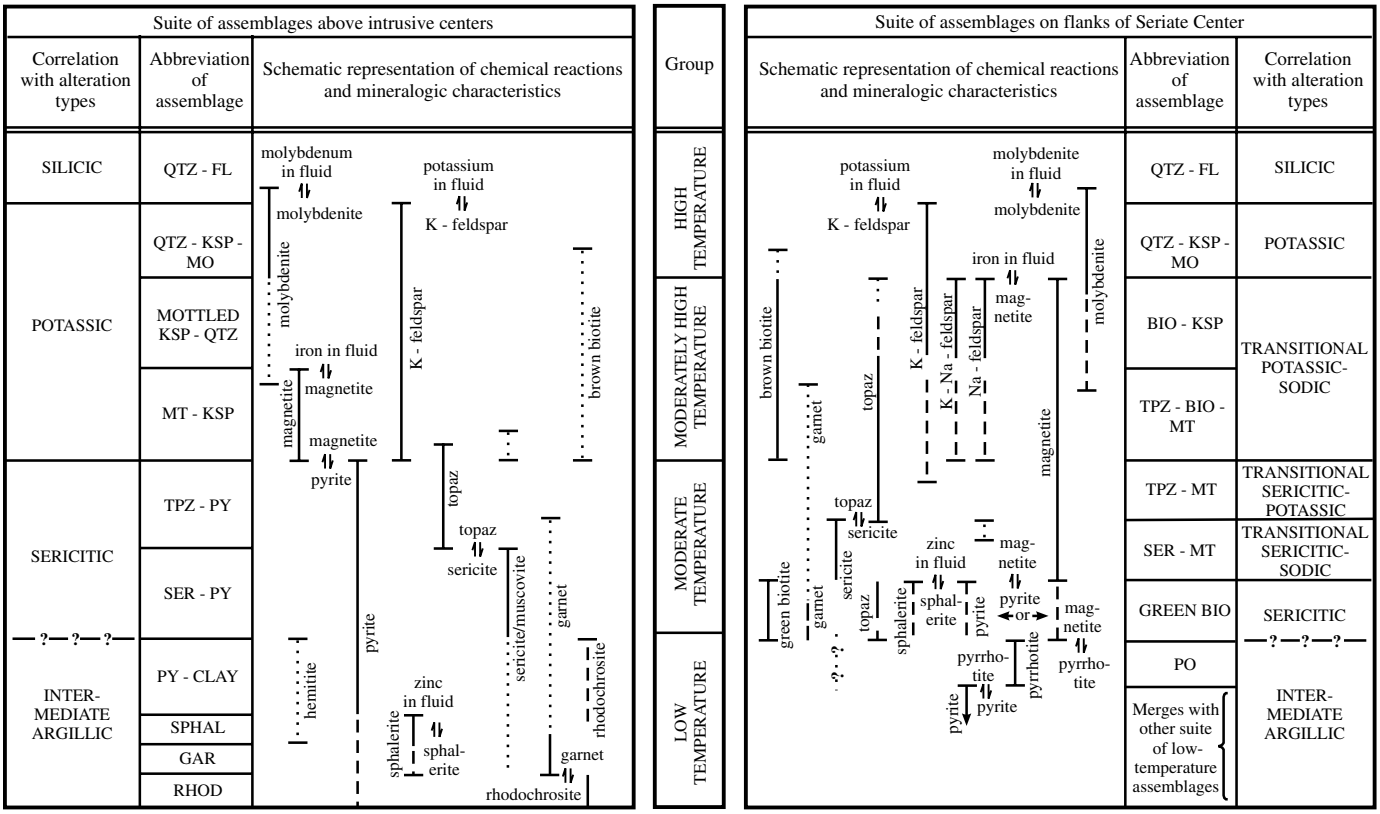

FIG. 7. Correlation of assemblages at Henderson with traditional terminology for types of alteration and schematic representation of selected chemical reactions and mineralogic characteristics of assemblages as a function of suite and temperature. At low temperatures, the two suites merge: low-temperature members of the suite that is most abundant above the Henderson and Seriate centers were superimposed on all assemblages that are restricted to the flanks of the Seriate center. The vertical distance that is assigned to any assemblage is arbitrary. Occurrences of selected minerals are labeled with vertical lettering. Minerals that are everywhere present in the assemblage are shown in solid lines; those that commonly are present are shown in dashed lines; and those that occur only locally are shown in dotted lines. Chemical reactions (labeled horizontally) encountered when moving from higher to lower parts of the diagram (from higher to lower temperature) correspond to those that would be observed along the path of a chemically and physically evolving fluid as it migrated across phase boundaries in a polythermal activity diagram. Such progressions, one for each side of the diagram, describe the two principal evolutionary paths of hydrothermal fluids with decreasing temperature. Deviations from this simplification of only two trajectories contribute to the inelegancies of the diagram (e.g., region near the GREEN BIO assemblage); these deviations are explicitly expressed by the paths shown in Figure 12.

to high-temperature mineral assemblages. No vein related to any lower temperature assemblage has been conclusively documented as cut off at such a contact anywhere in the Henderson mine.

At contacts between stocks of different intrusive centers (e.g., Primos stock in the Henderson center with Seriate stock in the Seriate center, Figs. 2A, 3C) and at contacts involving any of the 12 stocks related to the Henderson orebody with the enclosing Urad porphyry (Figs. 2A, 3A and C), certain lower temperature assemblages are cut off, albeit only at specific locations. The area around the top of the Henderson center was extensively exposed and mapped, but lower temperature assemblages are not cut off at contacts between any of the Henderson stocks and the Urad porphyry. The distribution and abundance of assemblages (Fig. 5B) and crosscutting relationships between various sets of veins (see below) suggest that moderately high temperature veins probably are locally cut off at the top of the East Lobe and Seriate stocks, although such a relationship was not definitively observed at an intrusive contact—perhaps because the top of the Seriate center is not as well exposed as the top of the Henderson center. In contrast, intrusions of the Vasquez center produced numerous, locally spectacular (Fig. 8G-H) examples of veins related to lower temperature assemblages cut off at intrusive contacts. Veins related to moderately high and moderate-temperature assemblages are cut off by the Vasquez stock and by Vasquez-related dikes that extend into Urad porphyry, as reflected in sharp truncations in the patterns of distribution of the associate mineral assemblages (Fig. 5B-C). Nonetheless, no veins related to low-temperature assemblages were observed cut off by intrusions from the Vasquez stock or any other intrusive contact in the deposit (Fig. 5D).

Crosscutting relationships between veins

Figure 8 shows photographs of representative crosscutting relationships, and the matrix of Figure 9 summarizes crosscutting vein relationships recorded during logging of drill

core throughout the deposit. The normal type of crosscutting relationship inferred to form by retrograde collapse of isotherms during cooling of intrusions includes two types: a younger vein cuts and offsets a vein related to a higher temperature assemblage, or a younger vein from the suite formed above intrusive centers cuts a vein related to an assemblage formed on the flanks of the Seriate center. The anomalous type of crosscutting relationship shows a reversal from the norm, i.e., a higher temperature vein cuts and offsets a lower temperature (or shallower) vein. Of more than 2,300 definitive crosscutting relationships recorded (Fig. 9), the anomalous ones represent only about 11 percent of the total, but they are critical to understanding the evolution of the system in time and space. Some anomalies represent small reversals, such as the QTZ-FL assemblage offsetting the QTZ-KSP-MO assemblage (both high-temperature assemblages), whereas other anomalies represent larger reversals, such as the QTZ-KSP-MO assemblage offsetting the SER-PY assemblage (high temperature offsetting moderate temperature).

The anomalous types of crosscutting relationships (Fig. 9) can be grouped into six types (Fig. 10), and the locations where such anomalous crosscutting relationships occur within the areas studied are restricted to certain regions of the deposit, as shown in the maps and cross sections of Figure 10. More than one-third of the drill holes logged have no anomalous relationship, whereas in certain parts of the deposit 20 to 50 percent of the crosscutting relationships logged is anomalous. Although it could be argued that the small reversals may not be significant, given that they involve assemblages in the same temperature groups (Table 1), the spatial restrictions to the small reversals (Fig. 10) suggest that even the small reversals may be recording important perturbations in the evolution of the hydrothermal system. Of the 260 anomalous relationships recorded, none involves any low-temperature assemblage (Figs. 9–10). In 232 of the 260 anomalous relationships recorded, the younger veinlet involves a high-temperature assemblage (compare anomalous types 1, 2, and 3 of Fig. 10 to Fig. 9).

Crosscutting relationships between veins provide timing information at numerous points in space, and the crosscutting contacts of individual intrusions provide markers to correlate spatially separated events. By integrating those data with the distribution of assemblages, the evolution of the hydrothermal system can be deduced.

Evolution in Time and Space

Frames of reference and displays of evolutionary paths

It is useful to explore alternate ways of representing the history of the hydrothermal system as functions of temperature, time, space, and the development of mineral assemblages. The conventional representation is a cross section showing the present distribution of alteration-mineralization products. Because this view is time integrated over the entire life of the hydrothermal system, however, it provides little insight into processes and dynamics. A second representation shows the progressive development of hydrothermal products in a series of time panels, but each panel remains an illustration of the cumulative development of alteration-mineralization products. Alternatively, one can use a series of time snapshots of the hydrothermal system, showing interpretations of where hydrothermal products were forming at various instants in time. A space-time diagram is complementary, as it displays time continuously by sacrificing one spatial dimension. All of the above displays use the rock as the frame of reference and a coordinate system that is fixed in space. Thus, these representations all adopt an Eulerian viewpoint in the nomenclature of fluid dynamics and transport theory (e.g., Shames, 1962, p. 72–73; Sissom and Pitts, 1972, p. 15 and 271; Lu, 1979, p. 205).

In porphyry systems, fluids range widely in temperature, pressure, and composition and operate on spatial scales of meters to kilometers, so a shift in frame of reference to the fluid perspective can provide valuable insights. When adopting the fluid perspective, the coordinate system is attached to a conceptual packet of moving fluid, rather than being fixed in space. This is the Lagrangian viewpoint of fluid dynamics. An evolutionary tree diagram is one means of explicitly displaying the evolution of the hydrothermal system from the fluid perspective.

We provide a variety of representations, utilizing both the rock and fluid perspectives, to model the complex evolutionary paths of the Henderson hydrothermal system.

Time frames

The descriptive model for Henderson employs 12 time frames of cross section 52N-N63E-58N (Fig. 11), each of which displays where fluids were flowing and reacting with rocks over short intervals of time at the deposit scale. By stripping off progressively older events using crosscutting relationships from offsetting veins and from veins that are cut off by younger intrusions (Figs. 5, 8–10), it is possible to identify regions where assemblages were forming during a particular time band. Time lines are generated at each intrusive contact that can be correlated across much of the deposit. From the field relationships at Henderson that indicate that high-temperature mineral assemblages developed virtually instantaneously after emplacement of each mineralizing stock within each intrusive center (Carten et al., 1988b, p. 291–293), it then follows that the spatial extent of the time lines can be effectively extended to the outer limit of the QTZ-KSP-MO assemblage (e.g., Fig. 11A, D, H). This can be done unambiguously in many parts of the Henderson deposit because of the simple geometrical distribution of veins related to the QTZ-KSP-MO assemblages and their relationship to the geometry of individual stocks and ore shells (e.g., Figs. 2–5). Note that all of the 12 frames of Figure 11 are quasi-instantaneous views that are not to be confused with cumulative time panels (e.g., Gustafson and Hunt, 1975, fig. 28).

After all stocks in the Henderson center had been emplaced and their associated ore shells had formed (Fig. 11A), but prior to the intrusion of the East Lobe and Seriate stocks of the Seriate center, first the MOTTLED KSP-QTZ assemblage and then the MT-KSP assemblage began to form above the Henderson center (Fig. 11B-C). This is evidenced by no lower temperature assemblages being cut off at any of the contacts between various stocks of the Henderson center and by the distribution of the MOTTLED KSP-QTZ assemblage being cut off by the East Lobe stock (Fig. 5B; compare Fig. 11B, D).

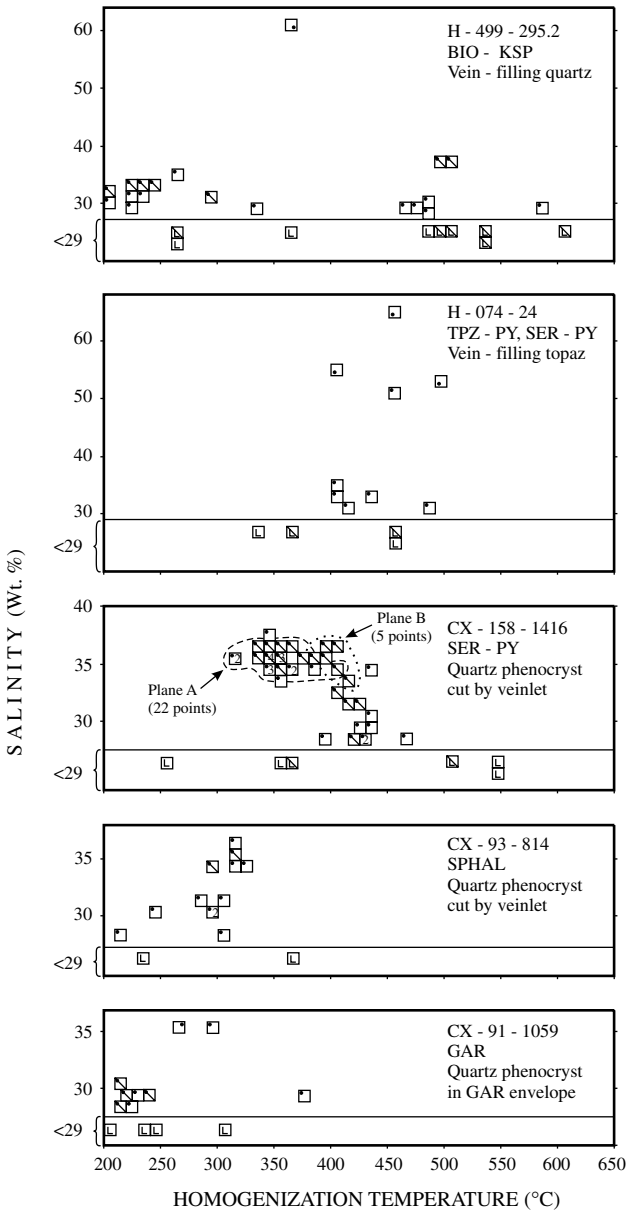
H - 499 - 295.2
BIO - KSP
Vein - filling quartz
H - 074 - 24
TPZ - PY, SER - PY
Vein - filling topaz
Plane B
(5 points)
Plane A
(22 points)
CX - 158 - 1416
SER - PY
Quartz phenocryst
cut by veinlet
CX - 93 - 814
SPHAL
Quartz phenocryst
cut by veinlet
CX - 91 - 1059
GAR
Quartz phenocryst
in GAR envelope
SALINITY (Wt. %)
HOMOGENIZATION TEMPERATURE (°C)

High-temperature veins related to stocks of the Seriate center (Fig. 11D) locally cut veins of the MOTTLED KSP-QTZ and MT-KSP assemblages related to the Henderson center, which created the type 2 anomalous relationship of Figure 10A-C. After intrusion of the stocks of the Seriate center, the suite of assemblages developed on the flanks of the Seriate center began to form (Fig. 11E). Concurrently at higher levels, the MOTTLED KSP-QTZ assemblage formed again and the MT-KSP assemblage also formed a zone over the Seriate center (Fig. 11E), as evidenced by development of anomalous relationship type 4 above the Seriate stock (Figs. 8B, 10A), and formation of second zones of concentration of each of the two assemblages that coalesce with their earlier zones (Fig. 5B; Table 7). The timing, restricted distribution, and unusual texture of the MOTTLED KSP-QTZ assemblage (Figs. 5B, 6A) suggest that it may record heating and boiling of preexisting brine, as predicted by Fournier (1999, p. 1199–1200), induced by emplacement of younger stocks and release of new batches of juvenile magmatic hydrothermal fluid. We infer from the spatial distribution of anomalous crosscutting relationships (Fig. 10) that the formation of the two MT-KSP zones probably overlapped in time, albeit beginning earlier over the Henderson center and perhaps persisting longer over the Seriate center (Fig. 11B-F).

Moderate-temperature assemblages first formed after all stocks of the Seriate center had been emplaced (Fig. 11F-G). The evidence that they did not form anywhere in the system before then includes the absence of anomalous crosscutting relationships types 3, 5, and 6 above an elevation of 7,900 ft (Fig. 10A-C). Specifically, crosscutting relationships indicate that neither of the two zones of the TPZ-PY assemblage (Fig. 5C; Table 7) began to form until after all stocks of the Seriate center had been emplaced (Fig. 11). Coupled with timing constraints on the initiation of alteration related to the TPZ-PY assemblage and the large extent of overlap in the distribution of the SER-PY and TPZ-PY assemblages (Fig. 5C), it follows that the two zones of concentration of the SER-PY assemblage (Fig. 5C; Table 7) did not begin to form anywhere in the system until after all stocks and associated ore shells were formed in both the Henderson and Seriate centers (Fig. 11G).

Emplacement of the Vasquez stock and formation of the Vasquez ore shell is an especially important time line (Fig. 11H) that generated a major reversal in the evolution of the system. Lower temperature assemblages that had developed on the flanks of the Seriate center are cut off by igneous rocks of the Vasquez center and are nowhere developed inside the Vasquez center (Figs. 4, 5B-C; 8C, F-H; 10A, D). In addition, numerous anomalous offsetting relationships of types 1, 2, and 3 were created above the Vasquez stock within the extent of high-temperature veins related to stocks of the Vasquez center (Figs. 8C-G; 10A-B, D).

FIG. 8. Photographs of crosscutting relationships between various veins and between intrusions and veins. Example of a normal offsetting relationship (see also Fig. 6A, D-E): A. A quartz-molybdenite vein (white arrow) of the QTZ-KSP-MO assemblage hosted by Urad porphyry is cut and offset by a vein with a vein filling and inner envelope of the TPZ-PY assemblage and an outer envelope of the SER-PY assemblage (delimited by black lines), i.e., a high-temperature vein offset by a moderate-temperature vein (sample H-321-335, located on section 480 H southeast of the aligned intrusions). Examples of anomalous offsetting relationships: B. K-feldspar-rich veinlet and alteration envelope (aligned black arrows) of the MOTTLED KSP-QTZ assemblage related to the Seriate center and hosted by Urad porphyry is superimposed on the MT-KSP assemblage related to the Henderson center, representing a slight reversal within moderately high temperature assemblages; note destruction of earlier deposited magnetite inside younger K-feldspar envelope (sample H-353-487, located on section 52N-N63E-58N between and slightly above the apices of the Henderson and Seriate centers). C. Quartz-molybdenite veinlet and associated K-feldspar envelope of the QTZ-KSP-MO assemblage related to the Vasquez center and hosted by Urad porphyry is superimposed on a veinlet of the TPZ-BIO-MT assemblage formed on the flanks of the Seriate center, representing a reversal from moderately high to high temperatures; note partial destruction (between black lines) of earlier deposited brown biotite inside K-feldspar envelope (sample H-497-1043.0, located at deep levels of section 480 H, southeast of the aligned intrusions). D. Sericitic alteration of the SER-PY assemblage related to the Seriate center and hosted by Urad porphyry cut and offset by a quartz-molybdenite veinlet (white arrow) and associated K-feldspar envelope (between black lines) of the QTZ-KSP-MO assemblage related to the Vasquez center, representing a reversal from moderate to high temperatures; note partial alteration of earlier sericite to K-feldspar within the envelope on the younger quartz-molybdenite veinlet (sample H-519-239.6, located due east of the Seriate center and above the Vasquez center). E. Sericitic envelope of the SER-PY assemblage on a pyritic vein that is subparallel to the photographed surface, which is related to the Seriate center and hosted by Urad porphyry, cut by two quartz-molybdenite veins of the QTZ-KSP-MO assemblage related to the Vasquez center, representing a reversal from moderate to high temperatures. Note that pinkish orange garnets (arrows with gt) occur along the outer alteration front (dashed black line) against fresh rocks and that the wider quartz-molybdenite vein at top has a K-feldspar envelope (solid black line) that is superimposed on the earlier sericitic envelope (sample H-519-239.6, located due east of the Seriate and above the Vasquez centers). F. Sericitic alteration envelope of the SER-MT assemblage, with magnetite partially sulfidized to pyrrhotite and pyrite, formed on the flanks of the Seriate center and hosted by Urad porphyry cut and offset by a quartz-molybdenite veinlet (white arrow) of the QTZ-KSP-MO assemblage related to the Vasquez center, representing a reversal from moderate to high temperatures (sample H-519-288.0, located due east of the Seriate center and above the Vasquez center). G. Sericitic alteration of the SER-MT assemblage, with magnetite partially sulfidized to pyrite, formed on the flanks of the Seriate center and hosted by Urad porphyry, cut by a dikelet from the Vasquez center. In turn, the dikelet is cut by a quartz vein (white arrows) of the QTZ-FL assemblage with an inner envelope of the QTZ-FL assemblage and an outer envelope of the QTZ-KSP-MO assemblage and by other veinlets (black arrows), all related to the Vasquez center; note that the inner silicic and outer potassic envelopes (delimited by black lines) destroy earlier sericitic alteration. The sample records a reversal from moderate to high temperatures (sample H-519-52, located due east of the Seriate center and above the Vasquez center). H. SER-MT assemblage formed on the flanks of the Seriate center and hosted by Urad porphyry cut off by a barren dike of the Vasquez center, representing truncation (black line) of moderate-temperature alteration assemblages by later magmatism related to the Vasquez center (sample H-451-766, located east of the Henderson center, south of the Seriate center, and above the Vasquez center).

Assemblage of Vein That Was Offset (Older)	Group	Mineral Assemblage (ABBREVIATION)	Assemblage of Offsetting Vein (Younger)																
		Group	High Temp		Mod High Temp				Moderate Temperature					Low Temperature					
	Group	Mineral Assemblage (ABBREVIATION)	QTZ-FL	QTZ-KSP-MO	BIO-KSP*	TPZ-BIO-MT*	MOTTLED KSP-QTZ	MT-KSP	TPZ-MT*	SER-MT*	GREEN BIO*	TPZ-PY	SER-PY	PO*	PY-CLAY	SPHAL	GAR	RHOD
	High Temp	QTZ-FL	29	122		2	7	5		1	1	7	31		2	2		2
		QTZ-KSP-MO	58	677	10	19	86	91	35	20	26	207	332		47	12	2	42
	Mod High Temp	BIO-KSP*	1	20	1	2		2										
		TPZ-BIO-MT*	1	71	1			12		2	1	1	1		2			
		MOTTLED KSP-QTZ		3				4				1	14		6			2
		MT-KSP	1	15			19			3	2	16	32		11	2		11
	Moderate Temperature	TPZ-MT*		42				2			2		1		1			4
		SER-MT*		14								2	2		1	5	2	
		GREEN BIO*									1							1
		TPZ-PY		1					4			3	19		1	4		10
		SER-PY		5					2				2			3	1	3
	Low Temperature	PO*																
		PY-CLAY														6		11
		SPHAL															1	7
		GAR																
		RHOD																

FIG. 9. Matrix of documented offsetting vein relationships (following Kutina, 1955, fig. 1, and Kamilli, 1986, fig. 13). Veins are ordered along the axes from high to low temperature; within each group, veins related to assemblages developed on the flanks of the Seriate center, denoted by asterisks (*) as in Table 1, are placed before veins generally formed above intrusive centers (i.e., deeper before shallower). Vein types of Table 2 are further simplified by classifying veins with zoned envelopes by the innermost assemblage (e.g., the vein-filling assemblage). Cells contain number of offsetting relationships between various permutations of veinlets recorded in logged drill holes; blank cells indicate no offsetting relationships observed. Matrix summarizes 2,300 observations; not shown in the matrix are an additional 58 crosscutting relationships of other types, such as those between dikes and between dikes and veins, and observations made in other types of samples. Relationships on the diagonal of the matrix from upper left to lower right pertain to veins of slightly different mineralogy that nonetheless belong to the same assemblage; in general, this shaded diagonal separates normal from anomalous crosscutting relationships. A normal crosscutting relationship (above and to the right of the diagonal) has a veinlet cut and offset by a veinlet of a lower temperature (or shallower) assemblage. An anomalous crosscutting relationship (those below the diagonal) represent a reversal in the typical sequence, where a veinlet of a higher temperature assemblage cuts and offsets a veinlet of a lower temperature (or shallower) assemblage.

As all stocks of the Vasquez center began to cool, a third zone of the MT-KSP assemblage—albeit small and mineralogically unusual—formed in and above the Vasquez stock (Fig. 5B; Table 7), but most moderately high and moderate-temperature assemblages are absent in the Vasquez center. Low-temperature assemblages, however, formed for the first time as the entire hydrothermal system waned (Fig. 11I-L).

Evidence from zoned alteration envelopes

Zoned alteration envelopes on veinlets are spectacularly developed during certain portions of the evolution of the Henderson system (Fig. 6E, G-H, K, Table 2), including at high temperature (Carten et al., 1988b, Fig. 12B). Evolutionary pathways are relatively straightforward to interpret from zoned envelopes. At the hand-specimen scale and under quasi-isothermal conditions, the fluid evolved from mineral assemblages stable in the inner zones (near the fluid channelway) to assemblages that are stable in outer zones (near the alteration front with fresh wall rocks). The high-temperature veinlets that exhibit inner silicic and outer potassic envelopes record a path from the QTZ-FL to the QTZ-KSP-MO assemblage. The moderate-temperature zoned envelopes indicate paths from the TPZ-MT to the SER-MT assemblage, from the TPZ-PY to the SER-PY assemblage, and from the

FIG. 10. Location of anomalous offsetting relationships recorded in logged drill holes in cross section and projected to plans. A. Bent cross section 52N-N63E-58N. B. Cross section 480 H. C. Points above elevation of 7,800 ft projected onto 8,100 level plan map and rectified with cross sections. D. Points below elevation of 7,800 ft projected onto 7,500 level plan map and rectified with cross sections. Both sections and plans show outline of 0.1 percent MoS_2 for reference (compare to Figs. 2–3; for section 480 H, see figs. 7 and 9 of Seedorff, 1988). Legend shows how offsetting relationships from matrix of Figure 9 are classified by temperature into six categories; note that some categories of relationships were not observed in certain plans and sections. As in Figure 9 and Table 1, veins related to assemblages developed on the flanks of the Seriate center are denoted by asterisks (*).

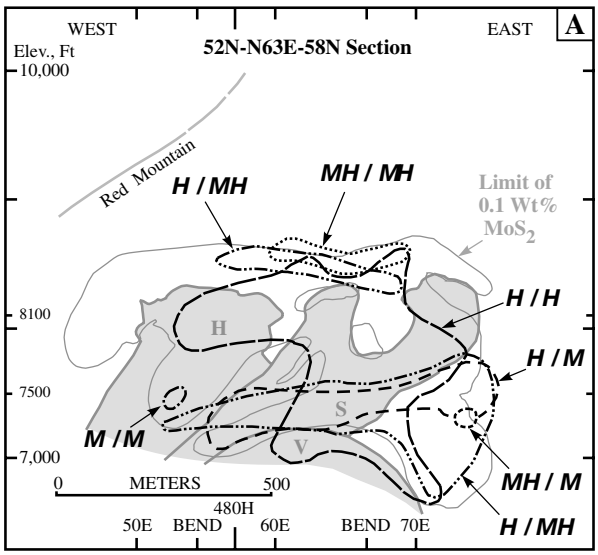

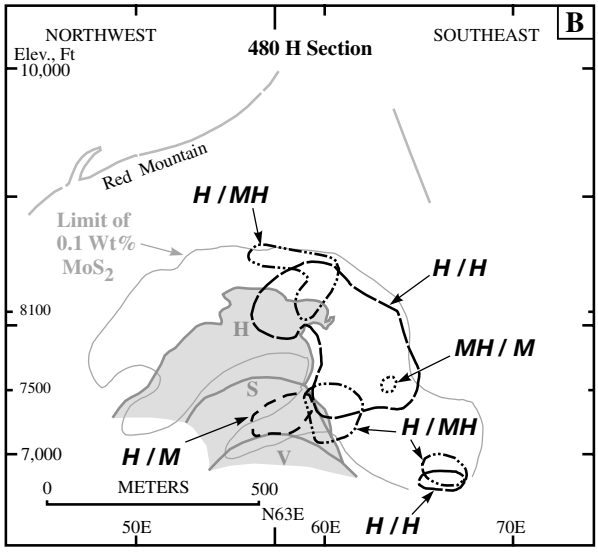

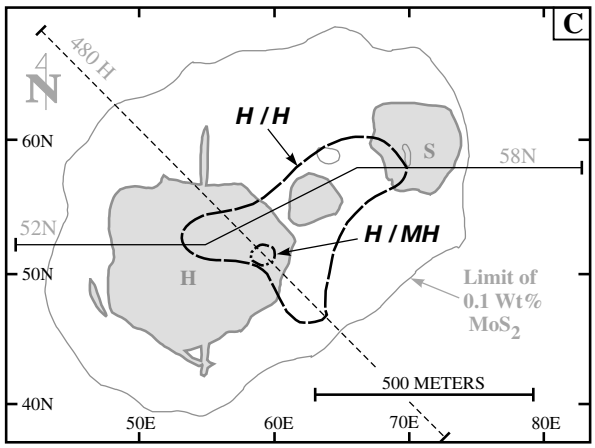

8100 LEVEL

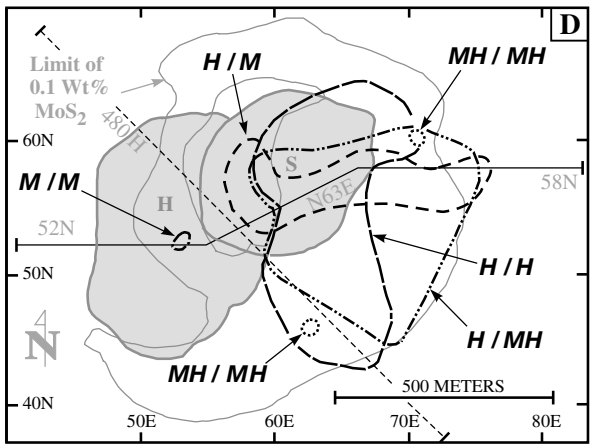

7500 LEVEL

LEGEND

Assemblage of Vein That Was Offset (Older) — Group	Mineral Assemblage (ABBREVIATION)	Assemblage of Offsetting Vein (Younger) — Group	QTZ-FL	QTZ-KSP-MO	BIO-KSP*	TPZ-BIO-MT*	MOTTLED KSP-QTZ	MT-KSP	TPZ-MT*	SER-MT*	GREEN BIO*	TPZ-PY	SER-PY	PO*	PY-CLAY	SPHAL	GAR	RHOD
High T	QTZ-FL	High T																
High T	QTZ-KSP-MO	High T	1															
Mod High T	BIO-KSP*	Mod High T	2															
Mod High T	TPZ-BIO-MT*	Mod High T	2					4										
Mod High T	MOTTLED KSP-QTZ	Mod High T	2					4										
Mod High T	MT-KSP	Mod High T	2					4										
Moderate Temp	TPZ-MT*	Moderate Temp	3															
Moderate Temp	SER-MT*	Moderate Temp	3					5										
Moderate Temp	GREEN BIO*	Moderate Temp	3					5										
Moderate Temp	TPZ-PY	Moderate Temp	3					5										
Moderate Temp	SER-PY	Moderate Temp	3					5										
Low Temperature	PO*	Low Temperature																
Low Temperature	PY-CLAY	Low Temperature																
Low Temperature	SPHAL	Low Temperature																
Low Temperature	GAR	Low Temperature																
Low Temperature	RHOD	Low Temperature																

Anomalous Offsetting Relationships

1 ——— High Temperature cuts High Temperature *(H / H)*

2 –·–·– High Temperature cuts Moderately High Temperature *(H / MH)*

3 – – – – High Temperature cuts Moderate Temperature *(H / M)*

4 ····· Moderately High Temperature cuts Moderately High Temperature *(MH / MH)*

5 ––––– Moderately High Temperature cuts Moderate Temperature *(MH / M)*

6 –·–·–· Moderate Temperature cuts Moderate Temperature *(M / M)*

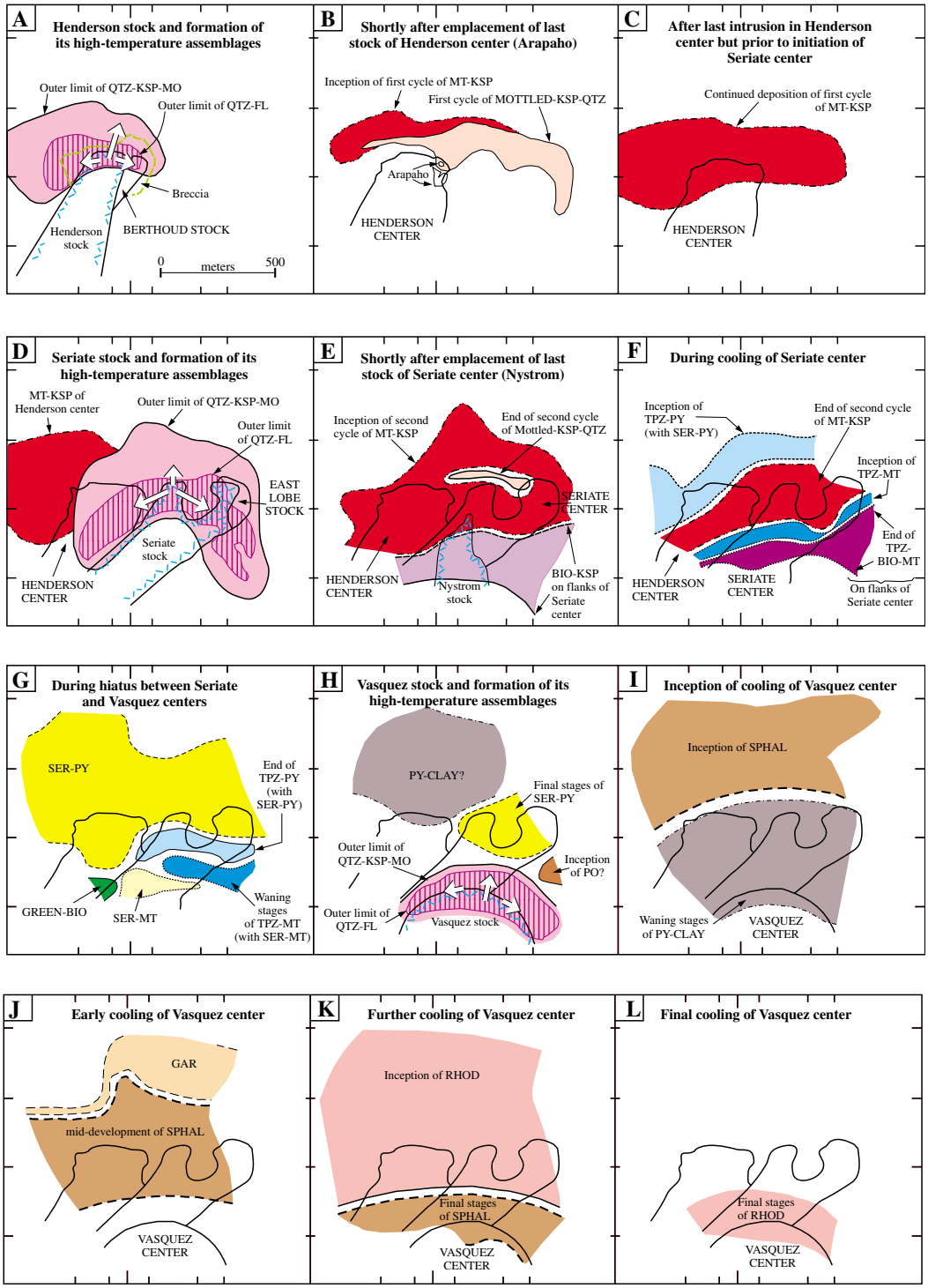

FIG. 11. Time frames showing progressive evolution of hydrothermal system on cross section 52N-N63E-58N. Each frame is limited to showing the distribution of assemblages formed, regardless of abundance, during a particular narrow interval of time (see bottom axis of Fig. 13). Tick marks (unlabeled) around borders of each panel correspond to labeled tick marks in Figures 2, 4–5, and 10. Both the tops and bottoms of the hydrothermal system are exposed in most panels. Assemblages and their abbreviations are defined in Table 1. Older intrusions are labeled in capital letters; intrusions that were emplaced shortly before a given time frame are ornamented near their margins and are labeled in lowercase letters. Lengths and orientations of white arrows in panels A, D, and H show direction and relative amounts of juvenile hydrothermal fluids released from the Henderson, Seriate, and Vasquez stocks, respectively, based on orientations and abundances of high-temperature veins (Carten et al., 1988b). Neither all assemblages nor all cycles of each assemblage are illustrated by these panels (e.g., a third cycle of MT-KSP would be between frames H and I). Relationships shown in panels E-G and the top half of H are consistent with crosscutting relationships at various points in space and present-day distributions, but there are no geologic time lines in this interval to provide better constraints.

TPZ-PY to the GREEN BIO assemblage. The suspected low-temperature zoned envelope suggests a path from the SPHAL to the GAR asemblage.

Zoned alteration envelopes record periods when fluids are relatively far from equilibrium with their wall rocks. As fluid flow persists along a channel way and the fluid continues to interact with its wall rocks (i.e., switching to the fluid perspective), one would expect inner envelopes to conceptually pinch out along the flow path, such that veins with zoned envelopes would be succeeded in time and space by veins displaying only the outer assemblage of the earlier veins. For example, veins with inner zones of the QTZ-FL assemblage and outer zones of the QTZ-KSP-MO assemblage would be succeeded by veins with only the QTZ-KSP-MO assemblage, or veins with zoned envelopes of the inner TPZ-PY and the outer SER-PY assemblages would be succeeded by veins with only the SER-PY assemblage. Indeed, these are the normal crosscutting relationships observed, and the reverse situations are the less common, anomalous relationships. This supports the argument above that the small reversals are significant and should not be discarded. (Of the anomalous reversals displayed in Figs. 9 and 10, only two small reversals involving the TPZ-PY assemblage cutting the SER-PY assembalge—versus 19 normal ones—are not readily accounted for by the descriptive model presented by the 12 time frames of Fig. 11). The succession of vein types indicates that the deposit-scale paths from high to low temperatures from the fluid perspective have segments that match the paths derived from zoned alteration envelopes.

Determination of deposit-scale paths

The evolutionary paths from the fluid perspective at the deposit scale can be described because the distribution of mineral assemblages and their succession as a function of space is known and general flow paths of fluids can be inferred (Figs. 5, 11). It is assumed that the distances that fluids migrate are relatively small during the transition from one mineral assemblage to the next youngest mineral assemblage (although the migration distance may be great when integrated across a number of successive assemblages). The evolutionary paths are deduced by integrating data from the spatial distributions of mineral assemblages formed at similar temperatures with the relative ages of the assemblages at various points in space (Figs. 9, 11), avoiding regions where reversals locally exist (Figs. 10–11). As an example, where the MOTTLED KSP-QTZ assemblage occurs around the Henderson center (Fig. 5B), it succeeds the QTZ-KSP-MO assemblage, which in turn is succeeded by the MT-KSP assemblage (Figs. 6A, 11A-C). This indicates a path between assemblages of QTZ-KSP-MO to MOTTLED KSP-QTZ to MT-KSP. Nonetheless, there is a large region above the Henderson center that lies above the uppermost occurrence of the MOTTLED KSP-QTZ assemblage where the QTZ-KSP-MO assemblage is succeeded directly by the MT-KSP assemblage (Figs. 5A-B,11A-C), which describes another path from QTZ-KSP-MO directly to MT-KSP, bypassing the MOTTLED KSP-QTZ assemblage.

An evolutionary tree diagram (Fig. 12) graphically depicts the deposit-scale evolutionary paths from the fluid perspective, including the segments described above. The diagram has coordinates of temperature and fluid evolution. The fluid evolution axis reflects time across most of the diagram, but this relationship is violated in detail. Note the segments that match the paths derived from zoned envelopes. Two principal trajectories are defined by the general succession of mineral assemblages in each of the two suites (inset of Fig. 12). Both suites evolve from a common set of high-temperature assemblages. For the suite that developed above intrusive centers, the evolutionary paths from the Henderson and Seriate centers merge as the two spatial zones of the MT-KSP assemblage merged. Spatial and temporal relationships indicate that at low temperatures the suite on the flanks of the Seriate center merged with the suite that is best developed above intrusive centers. The diagram similarly illustrates the merging of the Vasquez path with the previously merged Henderson-Seriate path during development of the PY-CLAY assemblage. This diagram conveys relationships between the principal evolutionary paths, describes the degree of cyclicity of deposition of lower temperature mineral assemblages, and incorporates the significant deviations that are observed from the two principal evolutionary paths. Note that the succession of assemblages locally bypasses some assemblages and that there are complex crossovers between the trajectories that define the two suites. High-temperature fluids derived from the Henderson, Seriate, and Vasquez stocks took progressively less time to reach equivalent points along their evolutionary paths. Heat and fluid added by stocks in later intrusive centers are interpreted to have contributed to slowing the rates of cooling and chemical evolution of earlier fluids.

The space-time diagram of Figure 13 (following Barton, 1982, fig. 35) shows only the vertical distribution of assemblages compared to the cross sectional display of Figure 11 but permits continuous display of the entire temporal range of evolution. Figure 13 shows the upper and lower limits of active alteration-mineralization and illustrates the vertical component of fluid-flow paths deduced from Figure 11. Allowing for its spatial limitations (e.g., the GREEN BIO assemblage is not present in the region through which the diagram is constructed), this diagram also depicts a portion of the complexity in paths described above, e.g., a path from QTZ-KSP-MO to MOTTLED KSP-QTZ to MT-KSP assemblages and a path directly from the QTZ-KSP-MO to the MT-KSP assemblage.

A more conventional display of space-time evolution is given in Figure 14 as a series of cumulative time panels (compare to fig. 28 of Gustafson and Hunt, 1975), as distinct from the quasi-instantaneous frames of Figure 11. The cumulative time panels provide a link to the familiar but are incapable of conveying the complex succession of mineral assemblages in time and space observed at Henderson and the evolutionary paths they record.

The upper and lower limits of the hydrothermal system, for much of its history, are preserved within the exposures mapped for this study (Figs. 11, 13). Due to the compact size and degree of exposure of the top of the Henderson system, it is possible to determine that sericitic alteration (Fig. 7) did not begin to form anywhere in the system until after intense potassic alteration (QTZ-KSP-MO assemblage) had terminated in the vicinity of stocks in both the Henderson and Seriate centers (Figs. 11–14). Further, veins of a late cycle of silicic (QTZ-FL assemblage) and intense potassic alteration

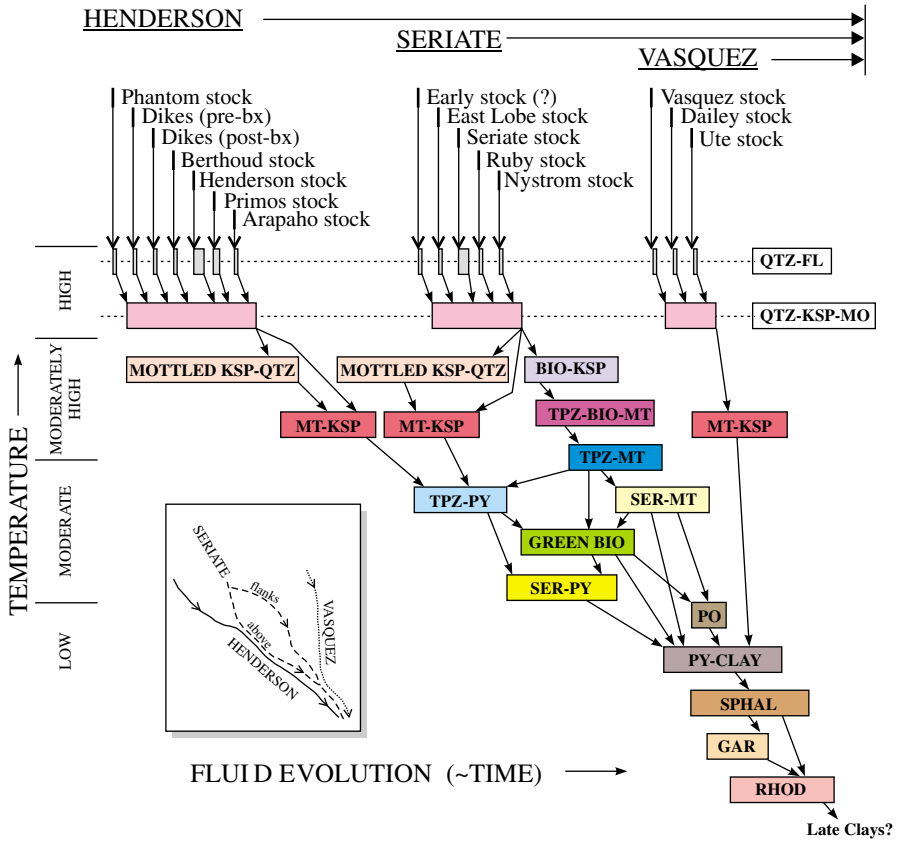
HENDERSON
SERIATE
VASQUEZ
Phantom stock
Dikes (pre-bx)
Dikes (post-bx)
Berthoud stock
Henderson stock
Primos stock
Arapaho stock
Early stock (?)
East Lobe stock
Seriate stock
Ruby stock
Nystrom stock
Vasquez stock
Dailey stock
Ute stock
HIGH
MODERATELY HIGH
MODERATE
LOW
TEMPERATURE
QTZ-FL
QTZ-KSP-MO
MOTTLED KSP-QTZ
MOTTLED KSP-QTZ
BIO-KSP
MT-KSP
MT-KSP
TPZ-BIO-MT
MT-KSP
TPZ-MT
TPZ-PY
SER-MT
GREEN BIO
SER-PY
PO
PY-CLAY
SPHAL
GAR
RHOD
Late Clays?
SERIATE
flanks
above
VASQUEZ
HENDERSON
FLUID EVOLUTION (~TIME)

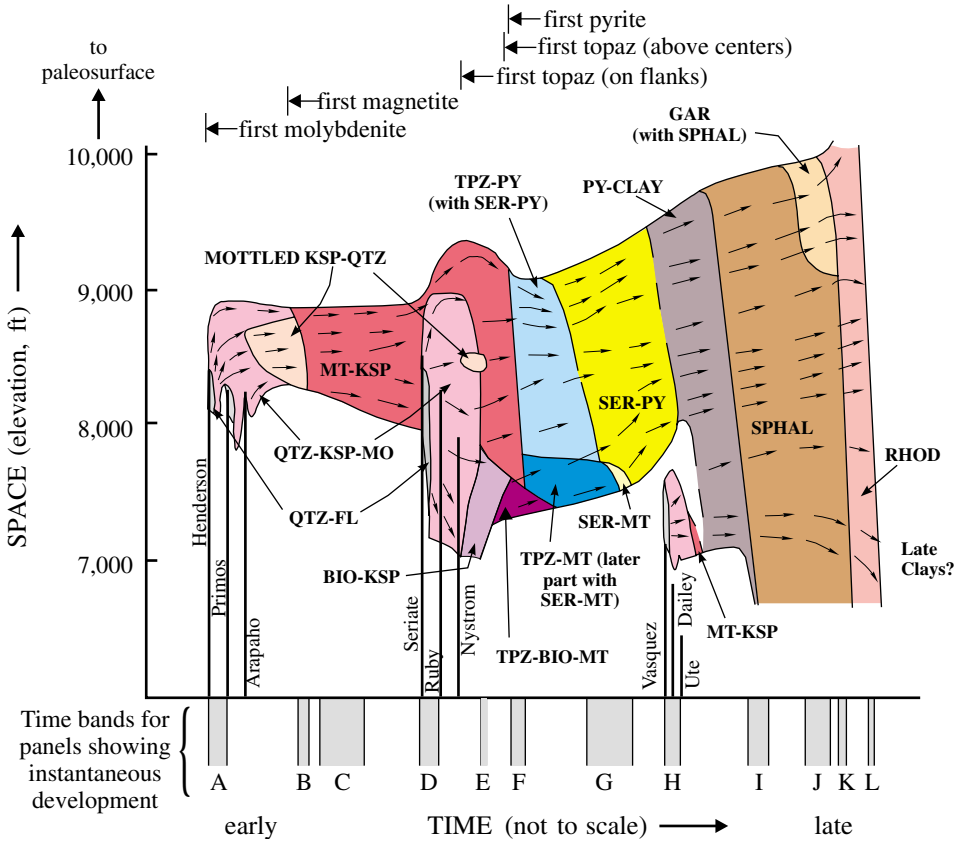
first pyrite
first topaz (above centers)
first topaz (on flanks)
first magnetite
first molybdenite
to paleosurface
10,000
9,000
8,000
7,000
SPACE (elevation, ft)
GAR (with SPHAL)
TPZ-PY (with SER-PY)
PY-CLAY
MOTTLED KSP-QTZ
MT-KSP
SER-PY
SPHAL
RHOD
QTZ-KSP-MO
QTZ-FL
SER-MT
Late Clays?
BIO-KSP
TPZ-MT (later part with SER-MT)
MT-KSP
TPZ-BIO-MT
Henderson
Primos
Arapaho
Seriate
Ruby
Nystrom
Vasquez
Dailey
Ute
Time bands for panels showing instantaneous development
A
B
C
D
E
F
G
H
I
J
K
L
early
TIME (not to scale)
late

(QTZ-KSP-MO assemblage) associated with the Vasquez stock locally cut and offset sericitic veinlets (Fig. 8D-G), as implied by Figures 11 to 13. In other well-studied deposits—especially porphyry copper systems—the great vertical extent of sericitic alteration to elevations well above presently preserved exposures and/or well above upper limits of high-temperature veins and alteration precludes determining the time of inception of sericitic alteration relative to potassic alteration. Because of the degree of exposure at the base of the Henderson system, it is also possible to establish that the deepest development of assemblages on the flanks of the Seriate center (Fig. 5) became slightly shallower with time (Figs. 11E-G, 13).

Figures 11 to 14 show that the vertical interval over which fluid-rock interaction produced visible alteration-mineralization products expanded significantly only during the development of low-temperature assemblages. While the region in which assemblages that are best developed over the Henderson and Seriate centers descended to significantly greater depths, collapsing on some assemblages of the suite on the flanks of the Seriate center (e.g., SER-PY in Figs. 11G, 13), the base of active fluid circulation continued to rise with time. At the time the Vasquez stock was emplaced, there may have been no lower temperature fluids present in the region where high-temperature assemblages related to the Vasquez stock were deposited (Figs. 11H, 13), although the SER-PY or PY-CLAY assemblages probably were forming at higher levels.

There is an absence of any anomalous offsetting relationships involving low-temperature assemblages, even between any pair of low-temperature assemblages (Figs. 9–10). Those relationships and the distribution of assemblages (Fig. 5) together require that the lines that bound most of the low-temperature assemblages on the space-time diagram (Fig. 13) be relatively steep. In other words, there probably were not a number of mineral assemblages forming in vertically stratified zones at any one time—perhaps only two low-temperature assemblages were forming at once anywhere in the system. For example, the RHOD assemblage is not abundant above the region where the GAR assemblage is abundant; in fact, the RHOD assemblage is abundant only at lower elevations than those where the GAR assemblage is abundant (Fig. 5D; Seedorff, 1988, figs. 25–26). Nonetheless, the RHOD assemblage postdates the GAR assemblage at any point (Figs. 12–13).

Despite the fact that each low-temperature assemblage was deposited in a single, late event, most low-temperature assemblages developed multiple zones of concentration, each crudely disposed about an intrusive center (Table 7; Fig. 5D). Each zone of concentration of the SPHAL assemblage, for example, reflects the sites where fluids were most abundant and where fractures were being formed at the time that a wave of deposition of the SPHAL assemblage (including the mineral sphalerite) gradually swept downward through the deposit (Figs. 11I-K–13). There is one zone of concentration for each general region where components apparently were introduced—the tops of the three intrusive centers—with the shallowest zone interpreted to be related to fluids from the Henderson center, the intermediate one related to the Seriate center, and the deepest one related to the Vasquez center (Fig. 5). The patterns are diffuse and formed at varying distances from the sites of introduction because fluids migrated between the time of introduction of components and the time

FIG. 12. Evolutionary tree for development of hydrothermal mineral assemblages, showing numerous high-temperature cycles, cyclical development of certain high- and moderately high temperature assemblages, and merging of evolutionary paths at low temperatures. The vertical axis is temperature, and the horizontal axis is fluid evolution, which is approximately equivalent to time throughout most of the diagram. Fluids evolve from high to low temperatures by following arrows along any of the paths from the top to the bottom of the diagram. The inset at lower left is a reduced view of paths across the same diagram, showing generalized trajectories of fluids from each intrusive center. The slopes of the trajectories qualitatively reflect cooling rates of fluids in different intrusive centers, fastest for Vasquez (steep trajectory) and slowest for Henderson (shallow trajectory). Cyclicity is indicated by the repetition of a given assemblages from left to right, e.g., numerous QTZ-FL and two for MOTTLED KSP-QTZ. Reversals are indicated when a relatively higher temperature assemblage begins to the right of a lower temperature assemblage, e.g., the high-temperature assemblage QTZ-FL associated with the East Lobe stock in the Seriate center occurs to the right of the moderately high temperature assemblage MOTTLED KSP-QTZ that formed from fluids that evolved from stocks of the Henderson center. The equivalence of the horizontal axis with time is violated in detail because of the geometrical difficulty in depicting fluids of similar temperature evolving at the same time both above and along the flanks of the Seriate center. The suite of assemblages that formed on the flanks of the Seriate assemblage is arbitrarily placed to the right of the suite of broadly contemporaneous assemblages that formed above the Seriate center. Fluids always evolve in the direction of the small arrows, even when the arrows point to the left (which would seem to point back in time). Linkages between the two suites create the complexities in the vicinity of the GREEN BIO assemblage box.

FIG. 13. Space-time diagram for evolution of mineral assemblages along a vertical line in the center of the hydrothermal system along bent cross section 52N-N63E-58N, between the two bends in the section that bound the N63E segment (Fig. 3). For the early history of the system (before intrusion of the Seriate stock), the location of the line is at the western end of the segment; thereafter, it is shifted slightly eastward such that it passes through the apex of the Seriate center, reflecting the shift in the center of hydrothermal activity. Black vertical bars represent essentially instantaneous emplacement and crystallization of stocks and associated release of magmatic fluids. The region between the upper and lower bounds of assemblages, with solid lines denoting mapped extent, represents the volume of rock where fluids were reacting with rocks to form visible alteration (presumably, relatively smaller volumes of fluid or reacted fluids were present beyond those limits). The arrows denote the inferred flow directions of fluids. The spacing of arrows along any vertical line is roughly proportional to the volume of alteration at any elevation at a given time, so that the density of arrows within an assemblage is proportional to the volume and reactivity of fluid in that region. The top of the diagram identifies the times at which selected minerals were first deposited. The shaded time bands along the bottom, labeled A through L, refer to time frames that show the quasi-instantaneous development of assemblages in Figure 11.

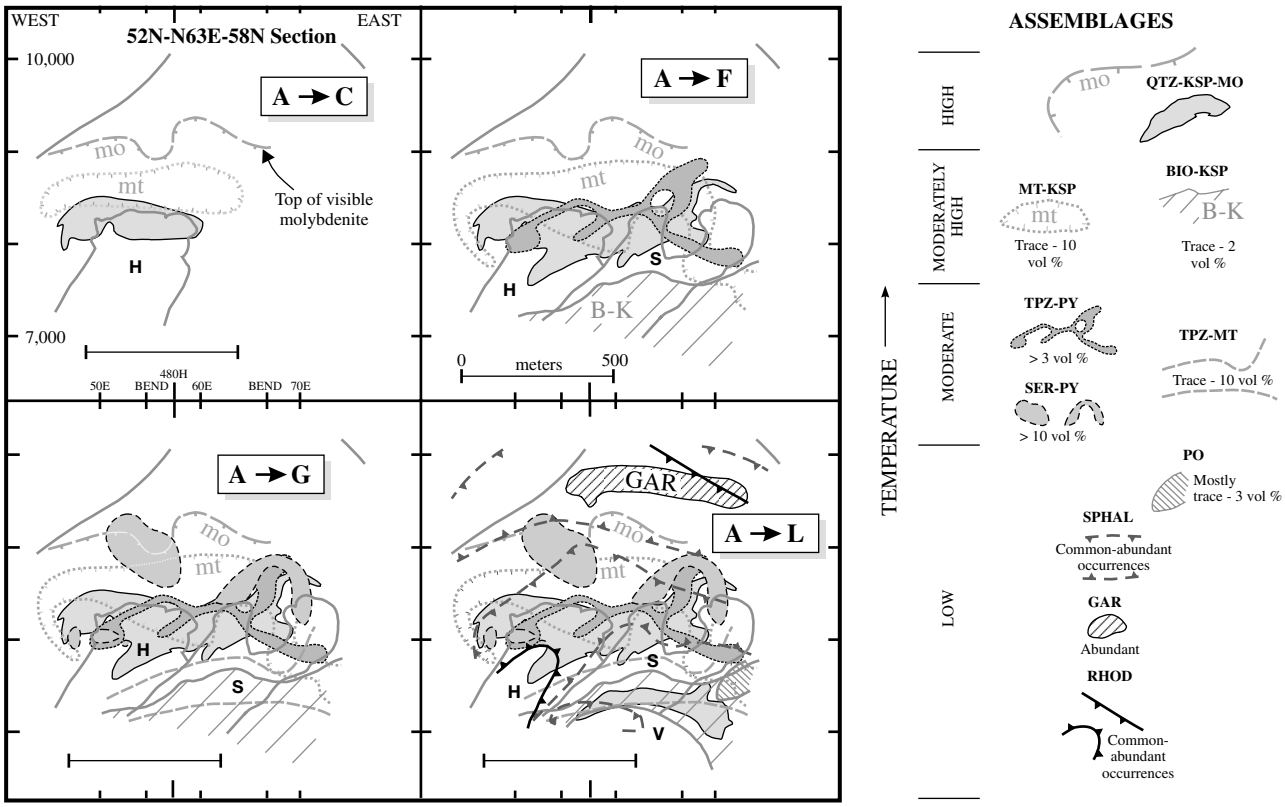

FIG. 14. Time-integrated view of progressive formation of Henderson along bent cross section 52N-N63E-58N, with panels showing cumulative development of selected hydrothermal mineral assemblages. The cumulative development of assemblages (abbreviations defined in Table 1) is tracked using the same letters that are used for the 12 time frames that show the instantaneous development of assemblages in Figure 11, which also are shown on the time axis of the space-time diagram of Figure 13. These four panels show the cumulative development from inception of the Henderson system in frame A of Figures 11 and 13, through frame C, through frame F, through frame G, and through the end of the Henderson system following frame L, respectively. Intrusive centers are identified by H (Henderson), S (Seriate), and V (Vasquez). The assemblages selected are the high-temperature assemblage QTZ-KSP-MO (principal host of Mo), the moderately high temperature assemblages MT-KSP and BIO-KSP, the moderate-temperature assemblages TPZ-PY (principal host of W), SER-PY (most important sericitic-type assemblage), and TPZ-MT, and the low-temperature assemblages PO, SPHAL (principal host of Pb-Zn), GAR (important host of Mn), and RHOD (other important host of Mn). In contrast to time slices of Figure 11, cumulative panels outline only specific abundance isopleths of selected assemblages (Fig. 5; see also Seedorff, 1988), as shown in the key.

of their deposition. The relative positions of each zone of concentration monitor the flow paths of fluids (Figs. 11–13). The paths, coupled with fluid inclusion evidence (Seedorff and Einaudi, 2004), indicate a lack of deposit-scale convective circulation in the development of assemblages described. Nonetheless, large-scale convection cannot be precluded for development of propylitic assemblages, which generally formed outside the region of this study (e.g., fig. 33 of White et al., 1981).

Figure 13 implies that hydrothermal alteration largely ceased in the region of study after deposition of the RHOD assemblage. Hence, either fluids became chemically less reactive or hydrothermal fluids were no longer present following deposition of this assemblage. Chemically reactive fluids present deep in the system during the late stages of alteration—the base of active fluid-rock reaction was dropping from the time of deposition of the PY-CLAY assemblage onward—could have exited out the top of the system if they had been neutralized by wall-rock reaction. An alternative explanation, preferred here, is that at least a fraction of the fluids sank into the Vasquez stock to form the late clay minerals or migrated laterally (a dimension not expressed in Fig. 13) out of the center of the system to the periphery. Lateral migration could have coincided with formation of small, scattered Ag-Pb-Zn–bearing carbonate veins that are peripheral to Red Mountain, such as the Puzzler mine (Fig. 1; Lovering and Goddard, 1950, p. 280–283), some of whose components were derived primarily from Henderson magmas (Stein and Hannah, 1985; Stein, 1988) and whose associated fluids are relatively saline, up to ~7 wt percent NaCl equiv (Corbetta, 1986). Drill hole exposure is not nearly as extensive laterally as it is vertically, so the evidence regarding this alternative—or any other potential lateral leakage—is inconclusive. Such a shift in the direction of fluid flow (and perhaps the initial decline in the base of fluid circulation during formation of the PY-CLAY assemblage; Fig. 13) could have been driven by emplacement of an intrusion somewhat distant from Red Mountain but related to the same underlying magma chamber. Such

intrusion(s) may not be exposed at the present surface or could include the intrusive center near Woods Mountain, 2.5 km southwest of Red Mountain (Fig. 1).

Discussion

Zones of concentration versus cycles of deposition

Many mineral assemblages at Henderson exhibit multiple zones of concentration, which reflect one or more depositional cycles. For high-temperature assemblages, there is a strict correlation between a given zone of concentration and a given cycle of deposition, which in turn coincide spatially and temporally with emplacement and crystallization of an individual stock (Table 7). For lower temperature assemblages, zones are spatially associated with intrusive centers, rather than with stocks. Moreover, multiple zones of a given lower temperature assemblage formed penecontemporaneously in a single event or cycle (Table 7).

Multiple ore shells and trace element halos are characteristic of porphyry molybdenum deposits (Wallace, 1974; White et al, 1981). At Henderson, mineral assemblages and their abundances are sufficiently well characterized and time lines are extensive enough to define the zones of concentration and establish their times of formation. Documentation of multiple zones of concentration are rare in porphyry copper systems (e.g., two, temporally distinct, vertically stacked couplets of potassic and sodic-calcic alteration at the Yerington porphyry copper mine; Carten, 1986), but they may be more common than presently recognized.

Distribution and abundance of sericitic alteration and timing of its inception

Several mineral assemblages compose sericitic alteration at Henderson (Fig. 7), but the SER-PY assemblage is volumetrically the most important (Fig. 5C; also fig. 18 of Seedorff, 1988). As previously described (e.g., Ranta et al., 1976; White et al., 1981), sericitic alteration is best developed above the Henderson orebody. The distribution of the SER-PY assemblage alteration, however, is less regular than previous depictions of a single bell-shaped volume; instead, the SER-PY assemblage alteration formed two, partially overlapping zones of concentration, one above the Henderson center and another above the Seriate center at a slightly lower elevation (Fig. 5C). Relative to the vast sea of sericitic alteration observed at many porphyry copper deposits, the volume of all sericitic-type assemblages at Henderson is moderate.

Past studies of porphyry systems have failed to establish direct evidence for the relative timing of potassic and sericitic alteration on the scale of the hydrothermal system rather than at given points in space (e.g., Gustafson and Hunt, 1975, p. 911), although numerous models have been proposed. These range from contemporaneous but zonally separated products (MacKenzie, 1970, p. 142, 144; Rose, 1970, p. 930; Hall et al., 1974, p. 898; Wallace et al., 1978, p. 361; Burnham, 1979, p. 131–132) to products formed at different times by different fluids (Sheppard et al., 1969, p. 771, 1971, p. 540; Sheppard and Gustafson, 1976, p. 1558). The field evidence at Henderson indicates that potassic and sericitic alteration were not contemporaneous products of spatially evolving or mixing hydrothermal fluids, as sericitic alteration did not begin to form at any level in the system until after intense potassic alteration associated with the Henderson and Seriate centers had terminated (Figs. 11–13). This is consistent with the general interpretation that there were few—rather than many—mineral assemblages forming in vertically stratified zones at any one time during the evolution of the hydrothermal system. Both potassic and sericitic assemblages formed above intrusive centers at Henderson from highly saline fluids of likely magmatic origin (Seedorff and Einaudi, 2004).

Fluid-flow paths and vertical extent of hydrothermal system

High-temperature magmatic hydrothermal fluids initially flowed out of the tops of stocks, whether the cause for apical release was extraordinary preemplacement enrichment in Mo and volatiles (Carten et al., 1988b), syncrystallization accumulation of fluid at the top of a convecting magma column (Shinohara et al., 1995), or another mechanism. Following apical release, hydrothermal fluids showed little net change in elevation during deposition of potassic and sericitic assemblages (Fig. 13). Most fluid released from stocks in the Henderson center flowed upward (Fig. 11A); however, a significant fraction of fluids that evolved from the apex of the Seriate stock was injected downward and outward (Fig. 11D), as indicated by the structural attitudes of veins (Carten et al., 1988b, Figs. 11, 16). This downward injection was caused by hydrothermal fluid pressures exceeding lithostatic pressures and may also be related to the unusual shape of the apex of the Seriate stock (Carten et al., 1988b). As these downward-injected fluids subsequently evolved, forming the distinct suite of assemblages best developed on the deep flanks of the Seriate center, the base of alteration-mineralization migrated upward (Fig. 13). The top and sides of the hydrothermal system expanded upward and outward, respectively, after all stocks of the Henderson and Seriate centers had been emplaced. The base of the reactive hydrothermal system finally descended at low temperatures after stocks of the Vasquez center had been emplaced (Figs. 11, 13). Considering limitations on drill exposure around the periphery at depth, fluids could have leaked out laterally over time, but the vertical interval over which the hydrothermal system was active expanded significantly only during the development of low-temperature, intermediate argillic assemblages (Figs. 11, 13).

The overall hydrothermal system has the appearance of a nonbuoyant, relatively stagnant reservoir where thermally and chemically evolving, saline hydrothermal fluid, for some time, reacted with a compact volume of rock, in spite of episodic, nearly instantaneous inputs of juvenile magmatic hydrothermal fluid as additional stocks were emplaced. New fractures formed continuously, bleeding off incrementally evolving fluids as earlier fractures were sealing as veinlets. The apparent lack of buoyancy may be attributed to the persistence of high salinities through time (Seedorff and Einaudi, 2004). The lack of large-scale convective circulation of fluids in development of the assemblages described here and supported by fluid inclusion evidence (Seedorff and Einaudi, 2004) suggests that many numerical models of fluid flow around heat sources (e.g., Norton, 1984) are not universally applicable to the relatively proximal, higher temperature, ore-forming stages in porphyry deposits. Although factors such as

the actual concentrations of components and the local storage capacity of fluids for the Henderson system are still poorly known, it is unclear at this time how constraints imposed by crosscutting relationships and spatial distributions of hydrothermal mineral assemblages (Figs. 2–5, 8–10) might be reconciled simultaneously with mass-balance issues.

Convective circulation of fluids, nonetheless, may be important at Henderson in development of propylitic alteration and veins at the periphery of the Dailey-Jones Pass mining district (Fig. 1). In some porphyry copper systems (e.g., Turquoise Gulch at El Salvador; Gustafson and Hunt, 1975), K silicate alteration and propylitic alteration are regarded as contemporaneous, zonally related products (proximal and distal, respectively) of Early alteration and mineralization. A zone of relatively fresh rocks separates both the high-temperature and the lower temperature assemblages from the first appearance of propylitic alteration at Henderson, which begs the question as to whether the flow paths of high- to low-temperature assemblages are linked to the paths of fluids that produced propylitic alteration. The origin of the white clay minerals of the lower argillic zone of MacKenzie (1970) and White et al. (1981) likewise remains a mystery.

Unidirectional versus cyclical evolutionary style

Early descriptive models of porphyry systems were concerned primarily with spatial relationships (e.g., Lowell and Guilbert, 1970), whereas later descriptions incorporated dynamic aspects (e.g., Gustafson and Hunt, 1975). In this latter context, the evolutionary style of a system can be considered perfectly cyclical if the entire range of high- to low-temperature mineral assemblages was deposited in sequence between emplacement of successive intrusions and if the sequence were repeated for each intrusion. In contrast, the evolutionary style can be considered perfectly unidirectional if mineral assemblages were deposited in an uninterrupted sequence from high to low temperatures, without reversals.

For the high-temperature portion of the Henderson system, hydrothermal fluids completed one cycle from silicic to potassic alteration after emplacement of each mineralizing stock and repeated the cycle once for each stock thereafter (Carten et al., 1988b). Fluids evolved to form lower temperature assemblages only during hiatuses between development of intrusive centers, not during the short intervals of time between emplacement of stocks of the same intrusive center. The evolutionary trend toward lower temperatures was reversed with each initiation of a new intrusive center (Figs. 11–13). The most marked reversal in this trend is evident where potassic veins associated with the late cycle of the Vasquez stock offset sericitic veinlets associated with an earlier composite Henderson-Seriate cycle (e.g., Fig. 8E-G). At the other extreme, represented by the low-temperature assemblages, the evolutionary style is approximately unidirectional, with each assemblage deposited in a single event (Table 7; Figs. 11–14). Hence, the Henderson system overall displays a variably cyclical evolutionary style. High-temperature fluids derived from stocks in the Henderson, Seriate, and Vasquez centers took progressively less time to reach equivalent points along their evolutionary paths (Figs. 12–13), in part because heat and fluids added by stocks in later intrusive centers slowed the rate of cooling of earlier fluids.

Implications for improved genetic models

The data presented for Henderson counter the claim (Ballard et al., 2001, p. 383) that field relationships cannot distinguish whether multiple igneous and hydrothermal events occurred during a single period of protracted magmatic-hydrothermal activity or as part of two or more discrete igneous-hydrothermal events that were superimposed. To the contrary, crosscutting relationships are key to evaluating geochronologic data regarding the lifespan of hydrothermal systems (Arribas et al., 1995; Henry et al., 1997; Marsh et al., 1997).

Current interpretations of geochronologic data from many porphyry-related deposits that call on long-lived systems are difficult to reconcile with observations on life spans and sizes of volcanoes and batholiths (e.g., Hildreth, 1981; Shaw, 1985; Sieh and Bursik, 1986; Hildreth and Lanphere, 1994) and commonly conflict with the life spans of porphyry-related hydrothermal systems predicted by thermal models (Cathles, 1981; Barton and Hanson, 1989; Hanson, 1996; Cathles et al., 1997; Marsh et al., 1997). The solution to the conundrum probably lies in undiscovered and/or undocumented field relationships. Clues for where to look may be found by seeking to determine the evolutionary style of each porphyry-related system, which can only be determined through documentation of the geology in four dimensions. Rigorous constraints on timing that are provided by crosscutting relationships, such as offsetting veins and of veins truncated by younger intrusions, are as important as three-dimensional patterns of rock type, structures, hydrothermal mineral assemblages, and metal grades. The temporal constraints are observed only during careful field mapping, logging, and petrography, with particular attention to unusual relationships. The understanding of porphyry deposits will have improved significantly when views developed from spatial patterns, crosscutting relationships, geochronology, and thermal models converge on mutually consistent interpretations.

The complexity and size of porphyry deposits necessitate better methods to record systematically and to synthesize field observations, such that descriptive models of deposits can be tested and readily utilized. Significant advances in understanding mineral deposits will depend on improving the quality and robustness of space-time models, ahead of or in parallel with advances in theory and analytical technology.

Conclusions

The fluorine-rich lower temperature mineral assemblages at Henderson commonly develop multiple zones of concentration, and these zones broadly envelop intrusive centers. Assemblages formed at higher temperatures tend to be deposited in multiple cycles, whereas those at lower temperatures were deposited in only a single event. We term this a variably cyclical evolutionary style. The lower temperature assemblages, which are well developed at high levels in the system and are thus of special interest to explorers, provide clues to the nature of the underlying molybdenum orebodies. At lower temperatures, however, the amplitude of the temporal record is dampened and the spatial patterns are more diffuse compared to the punctuated events and the sharply defined spatial patterns produced at high temperatures during emplacement and crystallization of individual

stocks. A companion paper (Seedorff and Einaudi, 2004) describes the associated geochemical evolutionary paths and decoupling of the introduction and deposition of metals at Henderson, with implications for genesis of porphyry deposits.

Acknowledgments

Decades of previous work by geologists at Henderson and Urad were invaluable to this study. In the context of this paper, contributions of Rick Carten, Matt Davidson, Ennis Geraghty, Bruce MacKenzie, Jim Shannon, Bruce Walker, and Will White were crucial, and we are honored to have shared in the excitement of some of their discoveries. It is a tribute to the character of Will White and Bob Kamilli that they welcomed us to build on their work, and Kamilli's examples led to Seedorff's routine use of offsetting vein matrices. Reviews of various sections and versions of the manuscript by Lew Gustafson, Bob Kamilli, Jean Cline, Mark Hannington, George Parks, Gail Mahood, Rick Carten, Mark Barton, Mark Sander, Dave John, Paul Zweng, Holly Stein, and David Maher are greatly appreciated. Discussions with Barton, Carten, John, Kamilli, Zweng, Paul Bartos, Dennis Bird, Don Burt, John Dilles, Dave Dobson, Phil Gans, Don Hudson, Jeff Keith, Larry Meinert, Rainer Newberry, Steve Olson, John Proffett, Mark Reed, Steve Shaver, and Holly Stein influenced our thinking. We were inspired by previous work in porphyry systems by Lew Gustafson, John Hunt, Stew Wallace, John Proffett, and Chuck Meyer. Frank Mazdab led the effort to calculate structural formulas from microprobe analyses; Mike Gutierrez drafted the figures; and Sandra Troutman analyzed clay minerals with the PIMA™ spectrometer. Barb Bekken, Gene Foord, Scott Manske, Debbie Montgomery, Jim Munoz, Julie Paque, and John-Mark Staude provided advice, favors, and technical assistance. Marianne Landtwing, Barton, Mazdab, and Staude are thanked for their roles in seeing the manuscript completed.

Financial support for this study came from: Climax Molybdenum Company, Western Operations, Golden, Colorado, under the leadership of Will White, Chief Geologist; National Science Foundation grant EAR-85-07264 to MTE; Chevron Fellowship, ASARCO research grant, and Mudd Fund in the Department of Applied Earth Sciences; and a travel grant from the Shell Companies Foundation to the School of Earth Sciences, Stanford University. We gratefully acknowledge Rick Carten, Will White, Bob Kamilli, and Arne Ward for lending their personal support to this project, especially during difficult economic times.

January 11, 2002; July 16, 2003

REFERENCES

Arancibia, O.N., and Clark, A.H., 1996, Early magnetite-amphibole-plagioclase alteration-mineralization in the Island Copper porphyry copper-gold-molybdenum deposit, British Columbia: Economic Geology, v. 91, p. 402–438.

Arribas, A., Jr., Hedenquist, J.W., Itaya, T., Okada, T., Concepción, R.A., and Garcia, J.S., Jr., 1995, Contemporaneous formation of adjacent porphyry and epithermal Cu-Au deposits over 300 ka in northern Luzon, Philippines: Geology, v. 23, p. 337–340.

Bailey, S.W., 1984, Classification and structures of the micas: Reviews in Mineralogy, v. 13, p. 1–12.

Ballard, J.R., Palin, J.M., Williams, I.S., Campbell, I.H., and Faunes, A., 2001, Two ages of porphyry intrusion resolved for the super-giant Chuquicamata copper deposit of northern Chile by ELA-ICP-MS and SHRIMP: Geology, v. 29, p. 383–386.

Barton, M.D., 1982, Some aspects of the geology and mineralogy of the fluorine-rich skarn at McCullough Butte, Eureka County, Nevada: Carnegie Institution of Washington Year Book, v. 81, p. 324–328.

Barton, M.D., and Hanson, R.B., 1989, Magmatism and the development of low-pressure metamorphic belts: Implications from the western United States and thermal modeling: Geological Society of America Bulletin, v. 101, p. 1051–1065.

Barton, M.D., Ilchik, R.P., and Marikos, M.A., 1991, Metasomatism: Reviews in Mineralogy, v. 26, p. 321–350.

Beane, R.E., 1983, The magmatic-hydrothermal transition: Geothermal Resources Council Special Report 13, p. 245–253.

Beane, R.E., and Bodnar, R.J., 1995, Hydrothermal fluids and hydrothermal alteration in porphyry copper deposits: Arizona Geological Digest, v. 20, p. 83–93.

Bright, M.J., 1974, Primary geochemical dispersion associated with the Henderson molybdenum deposit [abs.]: Economic Geology, v. 69, p. 1177.

Brimhall, G.H, Jr., 1980, Deep hypogene oxidation of porphyry copper potassium-silicate protore at Butte, Montana: A theoretical evaluation of the copper remobilization hypothesis: Economic Geology, v. 75, p. 384–409.

Burnham, C.W., 1979, Magmas and hydrothermal fluids, *in* Barnes, H.L., ed., Geochemistry of hydrothermal ore deposits, 2nd ed.: New York, John Wiley and Sons, p. 71–136.

Burnham, C.W., and Ohmoto, H., 1980, Late-stage processes of felsic magmatism: Mining Geology Special Issue 8, p. 1–11.

Burt, D.M., 1981, Acidity-salinity diagrams—applications to greisen and porphyry deposits: Economic Geology, v. 76, p. 832–843.

Campbell, A., and Petersen, U., 1988, Chemical zoning in wolframite from San Cristobal, Peru: Mineralium Deposita, v. 23, p. 132–137.

Carten, R.B., 1986, Sodium-calcium metasomatism: Chemical, temporal, and spatial relationships at the Yerington, Nevada, porphyry copper deposit: Economic Geology, v. 81, p. 1495–1519.

Carten, R.B., and Snee, L.W., 1995, Hydrothermal history and duration of ore formation at the Henderson porphyry molybdenum deposit, Colorado [abs.]: Geological Society of America Abstracts with Programs, v. 27, no. 6, p. A281.

Carten, R.B., Walker, B.M., Geraghty, E.P., and Gunow, A.J., 1988a, Comparison of field-based studies of the Henderson porphyry molybdenum deposit, Colorado, with experimental and theoretical models of porphyry systems: Canadian Institute of Mining and Metallurgy Special Volume 39, p. 351–366.

Carten, R.B., Geraghty, E.P., Walker, B.M., and Shannon, J.R., 1988b, Cyclic development of igneous features and their relationship to high-temperature hydrothermal features in the Henderson porphyry molybdenum deposit, Colorado: Economic Geology, v. 83, p. 266–296.

Carten, R.B., White, W.H., and Stein, H.J., 1993, High-grade granite-related molybdenum systems: Classification and origin: Geological Association of Canada Special Paper 40, p. 521–554.

Cathles, L.M., 1977, An analysis of the cooling of intrusives by ground-water convection which includes boiling: Economic Geology, v. 72, p. 804–826.

——1981, Fluid flow and genesis of hydrothermal ore deposits: Economic Geology 75th Anniversary Volume, p. 424–457.

Cathles, L.M., Erendi, A.H.J., and Barrie, T., 1997, How long can a hydrothermal system be sustained by a single intrusive event?: Economic Geology, v. 92, p. 766–771.

Cline, J.S., 1995, Genesis of porphyry copper deposits: The behavior of water, chloride, and copper in crystallizing melts: Arizona Geological Digest, v. 20, p. 69–82.

Cline, J.S., and Bodnar, R.J., 1991, Can economic porphyry copper mineralization be generated by a typical calc-alkaline melt?: Journal of Geophysical Research, v. 96, p. 8113–8126.

Corbetta, P.A., 1986, Geology of the Puzzler mine, Clear Creek County, Colorado: Unpublished M.S. thesis, Boulder, University of Colorado, 154 p.

Desborough, G.A., and Mihalik, P., 1980, Accessory minerals in the igneous host of molybdenum ore, Henderson mine, Colorado: U.S. Geological Survey Open-File Report 80-661, 16 p.

Dilles, J.H., and Einaudi, M.T., 1992, Wall-rock alteration and hydrothermal flow paths about the Ann-Mason porphyry copper deposit, Nevada—a 6-km vertical reconstruction: Economic Geology, v. 87, p. 1963–2001.

Dilles, J.H., Einaudi, M.T., Proffett, J., and Barton, M.D., 2000, Overview of the Yerington porphyry copper district: Magmatic to nonmagmatic sources of hydrothermal fluids: Their flow paths and alteration effects on rocks and Cu-Mo-Fe-Au ores: Society of Economic Geologists Guidebook Series, v. 32, p. 55–66.

Einaudi, M.T., 1977, Environment of ore deposition at Cerro de Pasco, Peru: Economic Geology, v. 72, p. 893–924.

——1982, Description of skarns associated with porphyry copper plutons, *in* Titley, S.R., ed., Advances in geology of the porphyry copper deposits, southwestern North America: Tucson, University of Arizona Press, p. 139–183.
Fournier, R.O., 1999, Hydrothermal processes related to movement of fluid from plastic into brittle rock in the magmatic-epithermal environment: Economic Geology, v. 94, p. 1193–1211.
Geissman, J.W., Snee, L.W., Graaskamp, G.W., Carten, R.B., and Geraghty, E.P., 1992, Deformation and age of the Red Mountain intrusive system (Urad-Henderson molybdenum deposits), Colorado: Evidence from paleomagnetic and $^{40}Ar/^{39}Ar$ data: Geological Society of America Bulletin, v. 104, p. 1031–1047.
Geraghty, E.P., Carten, R.B., and Walker, B.M., 1988, Tilting of Urad-Henderson and Climax porphyry molybdenum systems, central Colorado, as related to northern Rio Grande rift tectonics: Geological Society of America Bulletin, v. 100, p. 1780–1786.
Giggenbach, W.F., 1997, The origin and evolution of fluids in magmatic-hydrothermal systems, *in* Barnes, H.L., ed., Geochemistry of hydrothermal ore deposits, 3rd ed.: New York, John Wiley and Sons, p. 737–796.
Guilbert, J.M., and Lowell, J.D., 1974, Variations in zoning patterns in porphyry ore deposits: Canadian Institute of Mining and Metallurgy Bulletin, v. 67, no. 742, p. 99–109.
Gunow, A.J., 1983, Trace element mineralogy in the porphyry molybdenum environment: Unpublished Ph.D. dissertation, Boulder, University of Colorado, 267 p.
Gunow, A.J., Ludington, S., and Munoz, J.L., 1980, Fluorine in micas from the Henderson molybdenite deposit, Colorado: Economic Geology, v. 75, p. 1127–1137.
Gustafson, L.B., 1978, Some major factors of porphyry copper genesis: Economic Geology, v. 73, p. 600–607.
Gustafson, L.B., and Hunt, J.P., 1975, The porphyry copper deposit at El Salvador, Chile: Economic Geology, v. 70, p. 857–912.
Gustafson, L.B., and Quiroga G., J., 1995, Patterns of mineralization and alteration below the porphyry copper orebody at El Salvador, Chile: Economic Geology, v. 90, p. 2–16.
Gustafson, L.B., Orquera, W., McWilliams, M., Castro, M., Olivares, O., Rojas, G., Naluenda, J., and Mendez, M., 2001, Multiple centers of mineralization in the Indio Muerto district, El Salvador, Chile: Economic Geology, v. 96, p. 325–350.
Hall, W.E., Friedman, I., and Nash, J.T., 1974, Fluid inclusion and light stable isotope study of the Climax molybdenum deposits, Colorado: Economic Geology, v. 69, p. 884–901.
Hanson, R.B., 1996, Hydrodynamics of magmatic and meteoric fluids in the vicinity of granitic intrusions: Geological Society of America Special Paper 315, p. 251–259.
Harris, A.C., and Golding, S.D., 2002, New evidence of magmatic-fluid-related phyllic alteration: Implication for the genesis of porphyry Cu deposits: Geology, v. 30, p. 335–338.
Hedenquist, J.W., and Richards, J.P., 1998, The influence of geochemical techniques on the development of genetic models for porphyry copper deposits: Reviews in Economic Geology, v. 10, p. 235–256.
Hedenquist, J.W., Arribas, A., Jr., and Reynolds, T.J., 1998, Evolution of an intrusion-centered hydrothermal system: Far Southeast-Lepanto porphyry and epithermal Cu-Au deposits, Philippines: Economic Geology, v. 93, p. 373–404.
Helgeson, H.C., 1970, A chemical and thermodynamic model of ore deposition in hydrothermal systems: Mineralogical Society of America Special Paper 3, p. 155–186.
Henley, R.W., and McNabb, A., 1978, Magmatic vapor plumes and groundwater interaction in porphyry copper emplacement: Economic Geology, v. 73, p. 1–20.
Henry, C.D., Elson, H.B., McIntosh, W.C., Heizler, M.T., and Castor, S.B., 1997, Brief duration of hydrothermal activity at Round Mountain, Nevada, determined from $^{40}Ar/^{39}Ar$ geochronology: Economic Geology, v. 92, p. 807–826.
Hildreth, W., 1981, Gradients in silicic magma chambers: Implications for lithospheric magmatism: Journal of Geophysical Research, v. 86, p. 10,153–10,192.
Hildreth, W., and Lanphere, M.A., 1994, Potassium-argon geochronology of a basalt-andesite-dacite arc system: The Mount Adams volcanic field, Cascade Range of southern Washington: Geological Society of America Bulletin, v. 106, p. 1413–1429.
John, E.C., 1978, Mineral zones in the Utah Copper orebody: Economic Geology, v. 73, p. 1250–1259.
Kamilli, R.J., 1986, Genesis and evolution of the Baid al Jimalah tungsten deposit, Kingdom of Saudi Arabia: Saudi Arabia Ministry of Petroleum and Mineral Resources Technical Record USGS-TR-06-2 (IR 751), 54 p.
Kutina, J., 1955, Beitrag zur methodic der genetischen untersuchung von anschliffen in der erzmikroskopie: Chemie der Erde, v. 17, p. 176–180.
Lovering, T.S., and Goddard, E.N., 1950, Geology and ore deposits of the Front Range: U.S. Geologic Survey Professional Paper 223, 319 p.
Lowell, J.D., and Guilbert, J.M., 1970, Lateral and vertical alteration-mineralization zoning in porphyry ore deposits: Economic Geology, v. 65, p. 373–408.
Lu, P.-C., 1979, Fluid mechanics: An introductory course: Ames, Iowa State University Press, 468 p.
MacKenzie, W.B., 1970, Hydrothermal alteration associated with the Urad and Henderson molybdenite deposits, Clear Creek County, Colorado: Unpublished Ph.D. dissertation, Ann Arbor, University of Michigan, 208 p.
Marsh, T.M., Einaudi, M.T., and McWilliams, M., 1997, $^{40}Ar/^{39}Ar$ geochronology of Cu-Au and Au-Ag mineralization in the Potrerillos district, Chile: Economic Geology, v. 92, p. 784–806.
McMillan, W.J., and Panteleyev, A., 1995, Porphyry copper deposits of the Canadian Cordillera: Arizona Geological Society Digest, v. 20, p. 203–218.
Meyer, C., and Hemley, J.J., 1967, Wall rock alteration, *in* Barnes, H.L., ed., Geochemistry of hydrothermal ore deposits: New York, Holt, Rinehart, and Winston, p. 166–235.
Munoz, J.L., 1984, F-OH and Cl-OH exchange in micas with applications to hydrothermal ore deposits: Reviews in Mineralogy, v. 13, p. 469–493.
Muntean, J.L., and Einaudi, M.T., 2000, Porphyry gold deposits of the Refugio district, Maricunga belt, northern Chile: Economic Geology, v. 95, p. 1445–1472.
——2001, Porphyry-epithermal transition: Maricunga belt, northern Chile: Economic Geology, v. 96, p. 743–772.
Norton, D.L., 1982, Fluid and heat transport phenomena typical of copper-bearing pluton environments, *in* Titley, S.R., ed., Advances in geology of the porphyry copper deposits, southwestern North America: Tucson, University of Arizona Press, p. 59–72.
——1984, Theory of hydrothermal systems: Annual Reviews in Earth and Planetary Sciences, v. 12, p. 155–177.
Ossandón C., G., Fréraut C., R., Gustafson, L.B., Lindsay, D.D., and Zentilli, M., 2001, Geology of the Chuquicamata mine: A progress report: Economic Geology, v. 96, p. 249–270.
Peterman, Z.E., Hedge, C.E., and Braddock, W.A., 1968, Age of Precambrian events in the northeastern Front Range, Colorado: Journal of Geophysical Research, v. 73, p. 2277–2296.
Proffett, J.M., Jr., and Dilles, J.H., 1984, Geologic map of the Yerington district, Nevada: Nevada Bureau of Mines and Geology Map 77, scale 1:24,000.
Ranta, D.E., White, W.H., Ward, A.D., Graichen, R.E., Ganster, M.W., and Stewart, D.R., 1976, Geology of the Urad and Henderson molybdenite deposits—a review: Professional Contributions of Colorado School of Mines, no. 8, p. 477–485.
Rose, A.W., 1970, Zonal relations of wall-rock alteration and sulfide distribution at porphyry copper deposits: Economic Geology, v. 65, p. 920–936.
Rose, A.W., and Burt, D.M., 1979, Hydrothermal alteration, *in* Barnes, H.L., ed., Geochemistry of hydrothermal ore deposits, 2nd ed.: New York, John Wiley and Sons, p. 173–235.
Seedorff, E., 1986, Topaz in hydrothermal ore deposits: Advanced argillic, sericitic, or potassic alteration? [abs.]: Geological Society of America Abstracts with Programs, v. 18, p. 744.
——1987, Henderson porphyry molybdenum deposit: Cyclic alteration-mineralization and geochemical evolution of topaz- and magnetite-bearing assemblages: Unpublished Ph.D. dissertation, Stanford, California, Stanford University, 432 p.
——1988, Cyclic development of hydrothermal mineral assemblages related to multiple intrusions at the Henderson porphyry molybdenum deposit, Colorado: Canadian Institute of Mining and Metallurgy Special Volume 39, p. 367–393.
Seedorff, E., and Einaudi, M.T., 2004, Henderson porphyry molybdenum system, Colorado: II. Decoupling of introduction and deposition of metals during geochemical evolution of hydrothermal fluids: Economic Geology, v. 99, p. 37–70.
Shames, I.H., 1962, Mechanics of fluids: New York, McGraw-Hill, 558 p.
Shannon, J.R., Walker, B.M., Carten, R.B., and Geraghty, E.P., 1982, Unidirectional solidification textures and their significance in determining relative ages of intrusions at the Henderson mine, Colorado: Geology, v. 10, p. 293–297.

Shaver, S.A., 1991, Geology, alteration, mineralization and trace element geochemistry of the Hall (Nevada Moly) deposit, Nye County, Nevada, *in* Raines, G.L., Lisle, R.E., Schafer, R.W., and Wilkinson, W.H., eds., Geology and ore deposits of the Great Basin. Symposium Proceedings: Reno, Nevada, Geological Society of Nevada, v. 1, p. 303–332.

Shaw, H.R., 1985, Links between magma-tectonic rate balances, plutonism, and volcanism: Journal of Geophysical Research, v. 90, p. 11,275–11,288.

Shawe, D.R., Foord, E.E., and Conklin, N.M., 1984, Huebnerite veins near Round Mountain, Nye County, Nevada: U.S. Geological Survey Professional Paper 1287, 42 p.

Sheppard, S.M.F., and Gustafson, L.B., 1976, Oxygen and hydrogen isotopes in the porphyry copper deposit at El Salvador, Chile: ECONOMIC GEOLOGY, v. 71, p. 1549–1559.

Sheppard, S.M.F., Nielsen, R.L., and Taylor, H.P., Jr., 1969, Oxygen and hydrogen isotope ratios of clay minerals from porphyry copper deposits: ECONOMIC GEOLOGY, v. 64, p. 755–777.

——1971, Hydrogen and oxygen isotope ratios in minerals from porphyry copper deposits: ECONOMIC GEOLOGY, v. 66, p. 515–542.

Shinohara, H., Kazahaya, K., and Lowenstern, J.B., 1995, Volatile transport in a convecting magma column: Implications for porphyry Mo mineralization: Geology, v. 23, p. 1091–1094.

Sieh, K.E., and Bursik, M.I., 1986, Most recent eruption of the Mono Craters, eastern central California: Journal of Geophysical Research, v. 91, p. 12,539–12,571.

Sillitoe, R.H., 2000, Gold-rich porphyry deposits: Descriptive and genetic models and their role in exploration and discovery: Reviews in Economic Geology, v. 13, p. 315–345.

Sissom, L.E., and Pitts, D.R., 1972, Elements of transport phenomena: New York, McGraw-Hill, 814 p.

Smyth, J.R., Madel, R.E., McCormick, T.C., Munoz, J.L., and Rossman, G.R., 1990, Crystal-structure refinement of an F-bearing spessartine garnet: American Mineralogist, v. 75, p. 314–318.

Stein, H.J., 1988, Genetic traits of Climax-type granites and molybdenum mineralization, Colorado mineral belt: Canadian Institute of Mining and Metallurgy Special Volume 39, p. 394–401.

Stein, H.J., and Crock, J.G., 1990, Late Cretaceous-Tertiary magmatism in the Colorado mineral belt: Rare earth element and samarium-neodymium isotopic studies: Geological Society of America Memoir 174, p. 195–223.

Stein, H.J., and Hannah, J.L., 1985, Movement and origin of ore fluids in Climax-type systems: Geology, v. 13, p. 469–474.

Taylor, H.P., Jr., 1997, Oxygen and hydrogen isotope relationships in hydrothermal mineral deposits, *in* Barnes, H.L., ed., Geochemistry of hydrothermal ore deposits, 3rd ed.: New York, John Wiley and Sons, p. 229–302.

Titley, S.R., and Beane, R.E., 1981, Porphyry copper deposits, Part I. Geologic settings, petrology, and tectogenesis: ECONOMIC GEOLOGY 75TH ANNIVERSARY VOLUME, p. 214–235.

Ulrich, T., Günther, D., and Heinrich, C.A., 2001, The evolution of a porphyry Cu-Au deposit, based on LA-ICP-MS analysis of fluid inclusions: Bajo de la Alumbrera, Argentina: ECONOMIC GEOLOGY, v. 96, p. 1743–1774; corrected version, 2002, v. 97, p. 1889–1920.

van Middelaar, W.T., and Keith, J.D., 1990, Mica chemistry as an indicator of oxygen and halogen fugacities in the CanTung and other W-related granitoids in the North American Cordillera: Geological Society of America Special Paper 246, p. 205–220.

Wallace, S.R., 1974, The Henderson ore body—elements of discovery, reflections: American Institute of Mining, Metallurgical, and Petroleum Engineers Transactions, v. 256, p. 216–227.

——1995, Presidential address: The Climax-type molybdenite deposits: What they are, where they are, and why they are: ECONOMIC GEOLOGY, v. 90, p. 1359–1380.

Wallace, S.R., Muncaster, N.K., Jonson, D.C., MacKenzie, W.B., Bookstrom, A.A., and Surface, V.E., 1968, Multiple intrusion and mineralization at Climax, Colorado, *in* Ridge, J.D., ed., Ore deposits of the United States, 1933–1967 (Graton-Sales volume): New York, American Institute Mining Metallurgy and Petroleum Engineers, v. 1, p. 605–640.

Wallace, S.R., MacKenzie, W.B., Blair, R.G., and Muncaster, N.K., 1978, Geology of the Urad and Henderson molybdenite deposits, Clear Creek County, Colorado, with a section on a comparison of these deposits with those at Climax, Colorado: ECONOMIC GEOLOGY, v. 73, p. 325–368.

Watanabe, Y., and Hedenquist, J.W., 2001, Mineralogic and stable isotope zonation at the surface over the El Salvador porphyry copper deposit, Chile: ECONOMIC GEOLOGY, v. 96, p. 1775–1797.

White, W.H., Bookstrom, A.A., Kamilli, R.J., Ganster, M.W., Smith, R.P., Ranta, D.E., and Steininger, R.C., 1981, Character and origin of Climax-type molybdenum deposits: ECONOMIC GEOLOGY 75TH ANNIVERSARY VOLUME, p. 270–316.

Zhang, L., Dilles, J.H., Field, C.W., and Reed, M.H., 1999, Oxygen and hydrogen isotope geochemistry of pre-Main Stage porphyry Cu-Mo mineralization at Butte, Montana [abs.]: Geological Society of America Abstracts with Programs, v. 31, no. 7, p. A381.